### REVIEW ARTICLE







Check for updates

# Short fiber reinforcement in material extrusion 3D printing: A meta-analysis review with insights into sustainable alternatives

Csenge Tóth<sup>1,2</sup> | Kolos Molnár<sup>1,3</sup> | Ábris Dávid Virág<sup>1</sup>

<sup>1</sup>Department of Polymer Engineering, Faculty of Mechanical Engineering, Budapest University of Technology and Economics, Budapest, Hungary

<sup>2</sup>Department of Polymer Engineering, MTA-BME Lendület Lightweight Polymer Composites Research Group, Budapest, Hungary

<sup>3</sup>Department of Polymer Engineering, HUN-REN-BME Research Group for Composite Science and Technology, Budapest, Hungary

## Correspondence

Kolos Molnár, Department of Polymer Engineering, Faculty of Mechanical Engineering, Budapest University of Technology and Economics, Műegyetem rkp. 3. H-1111, Budapest, Hungary. Email: molnar@pt.bme.hu

### Funding information

National Research, Development and Innovation Fund; János Bolyai Scholarship of the Hungarian Academy of Sciences; National Research, Development and Innovation Office (NRDI, Hungary), Grant/Award Numbers: K146236, FK138501; Ministry of Culture and Innovation of Hungary from the National Research, Development and Innovation Fund

### **Abstract**

Short fiber reinforcement is a key for improving the mechanical properties of thermoplastic composites produced by 3D printing. However, the strengthening potential of fibers is often under-utilized due to sub-optimal processing conditions. This meta-analysis review systematically evaluates the microstructural and mechanical properties of short fiber-reinforced composites, identifying key trends related to fiber fragmentation, fiber-matrix interactions, and property optimization. Our statistical analysis results show that fiber content and initial fiber length have minimal effect on the average remaining fiber length in the filament, which highlights that processing conditions are the primary control on fiber breakage. In addition, the fiber aspect ratio does not show a direct correlation with tensile strength, which can be due to insufficient fiber-matrix adhesion. Despite these drawbacks, the fibers still increase the tensile modulus by an average of 2.22 times and the flexural modulus by an average of 2.69 times. Analytical models for predicting mechanical properties are also presented, noting that while they provide valuable insights, time-consuming experimental validation is still required for accurate estimates. Finally, we provide insights into sustainable waste-derived fillers as potential alternatives to conventional fibers. Although their mechanical performance remains less predictable, surface treatment strategies and advanced multi-scale modeling techniques will be essential to establish structure-property relationships and to exploit their potential fully. Ultimately, waste-derived fillers hold significant promise for replacing raw material from primary sources, paving the way for more sustainable composite 3D printing.

### **Highlights**

- Waste-derived fillers are emerging in 3D-printed composites.
- · Improved micromechanical models are needed to predict the effects of waste fillers.
- Statistical analysis shows that tensile strength is independent of aspect ratio.
- Filler content does not affect fragmentation during filament manufacturing.

This is an open access article under the terms of the Creative Commons Attribution-NonCommercial License, which permits use, distribution and reproduction in any medium, provided the original work is properly cited and is not used for commercial purposes.

© 2025 The Author(s). Polymer Composites published by Wiley Periodicals LLC on behalf of Society of Plastics Engineers.

15480569, 0, Downloaded from https://4spepublications.onlinelibrary.wiley.com/doi/10.1002/pc.29850 by Budapest University of Technology and Economics, Wiley Online Library on [21/08/2025]. See the Terms and Conditions (https://onlinelibrary.

of use; OA articles are governed by the applicable Creative Commons

### KEYWORDS

mechanical modeling, microstructure, short fiber composite, sustainable composites, waste fillers

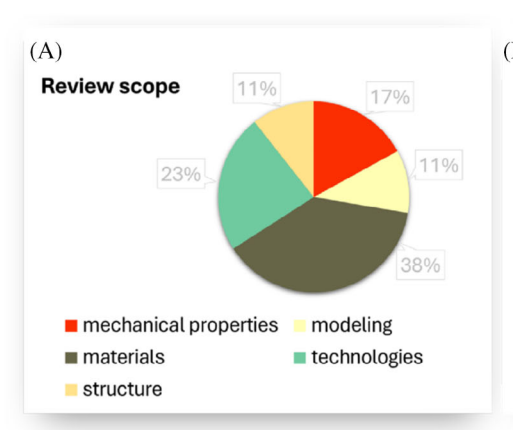
### 1 | INTRODUCTION

Since their introduction in 1987, 3D printing techniques have received considerable attention and revolutionized manufacturing and design. According to ISO/ASTM 52900:2015, material extrusion (MatEx), or generally referred to as Fused Filament Fabrication (FFF) is an additive manufacturing process in which the material is selectively fed through a nozzle or orifice. In this article, the abbreviation FFF is used specifically to refer to the process using a thermoplastic filament. During the printing process, the filament is passed through a heated nozzle, which melts it, and the material is deposited along a preprogrammed path. The process continues layer by layer, with each layer cooling and solidifying as the object takes shape, creating complex geometries and customized material properties in a single manufacturing step. 2,3

In the field of FFF 3D printing, there has been a significant increase in scholarly attention, as evidenced by the publication of more than 50 review articles over the past 5 years. The primary focus areas can be categorized into five main topics: mechanical properties, materials, structures, technologies, and modeling (Figure 1A). Most of the reviews center around the materials used (38%), with more and more sustainable alternatives emerging. The second most frequently discussed topic is the variety of technologies (23%), with a focus on how different printing methods and equipment innovations affect performance. Reviews focusing on mechanical properties

account for 17% of all articles processed. The least reviewed areas are modeling and simulation (11%), which aim to predict and optimize the mechanical performance of 3D-printed parts, and the structure (11%), in which the microstructural features are collected and analyzed. Based on the www.sciencedirect.com database, the number of articles on short-fiber composites or the prediction of mechanical properties of 3D printed parts has increased exponentially over the last 10 years (Figure 1B). In 2023, the number of research articles on 3D printing was 10,053, of which 1132 focused on short-fiber composites and 1458 on the prediction of mechanical properties.

The combination of material extrusion 3D printing and fiber reinforcement opens up many advantages and innovation opportunities, with unique properties for a wide range of applications. The expected benefits of fiber-reinforced thermoplastics are the increased mechanical properties and the unique geometric possibilities achieved with 3D printing. The thermoplastic polymer matrix ensures easy recyclability, and the technology allows for a wide range of material combinations, opening up the possibility of using bio-based and/or recycled materials and natural fibers. Wastederived fillers are also emerging, as many materials that cannot be recycled on their own can be recycled as fillers when mixed into the thermoplastic matrix. Therefore, FFF 3D printing of thermoplastic composites can offer a sustainable alternative in many industries. With the use of biocompatible materials, patient-specific



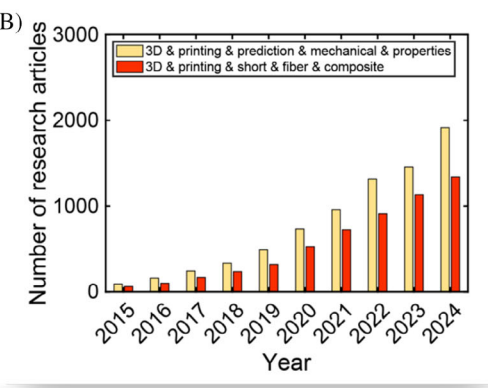


FIGURE 1 (A) Reviews in the topic of Material Extrusion 3D printing from the past 5 years and the general scope of the reviews<sup>2–47</sup> (B) The number of articles found with the following keywords: 3D printing, prediction, mechanical properties, and 3D printing, short fiber, composite based on the www.sciencedirect.com database.

implants or surgical tools can be manufactured to fit individual patient anatomy. 48-51 By using lattice or honeycomb structures, lightweight structural elements can be produced that are beneficial to the automotive and aerospace industries. 52-54 The use of functional fillers such as carbon fibers, carbon nanotubes, or metal particles allows the production of smart composite materials. Electrically conductive composites are applied for sensors, 55,56 soft robotic components or electromagnetic interference shielding, <sup>59,60</sup> and thermally conductive 3D-printed composites can be beneficial for custom heat sinks or cooling systems. 61,62

Both short and continuous fibers can be used as reinforcement for FFF 3D printing, and these have different advantages and different applications. Unlike continuous fibers, short fiber composites do not require any special equipment for 3D printing, and the filament containing the fibers can be processed on any desktop equipment. As a result, these materials are more accessible, and many research projects use self-developed composites. However, our review shows that in many cases, the reinforcing effect of short fibers is not exploited, and predictive methods are not well applied. Consequently, the aim of this review is to assist the design of short fiber composites by providing an overview of microstructural properties, statistical analysis of expected mechanical properties, and the application of micromechanical models.

In most cases, FFF 3D printing starts from a filament, so a pre-processing step is necessary to compound and shape the reinforcement and the matrix. Therefore, the materials undergo at least two processing steps, during which they are subjected to cyclic thermal stress and shear loads. Repeated stress inevitably causes degradation, which can appear in the decrease in the molecular weight of the matrix or in the fragmentation of the reinforcing fibers. 63-65 The widely acclaimed advantage of 3D printing is the ability to create unique geometries, which is made possible by the many freely adjustable manufacturing parameters. However, this degree of freedom also means that the microstructural properties of 3D printed products vary greatly depending on the parameters. Knowledge of microstructural features is important for the prediction of mechanical properties. Many predictive methods used for thermoplastic composites are empirical, relying on experimentally derived data and relationships to forecast material behavior. The empirical or semi-empirical methods (e.g., Halpin-Tsai, Cox, and Mori-Tanaka, etc.) involve creating mathematical models based on observed trends in composite behavior under various conditions, such as fiber orientation and fiber length. This systematic review aims to collect observed trends in the literature and identify further trends through meta-analysis. We analyze the relationship between the processing parameters and the

microstructure and between the microstructure and the mechanical properties. We discuss and identify the use of microstructural features in mechanical modeling, and overall, the analysis provides general conclusions on the current advantages and limitations of 3D-printed short fiber-reinforced thermoplastic composites.

#### 2 STATISTICAL METHODOLOGY

We used the Minitab 21.1.0 statistical software (Minitab LLC, State College, PA) and the Statistics and Machine Learning Toolbox of Matlab R2022a (Mathworks, Natick, MA) for statistical analysis. Before performing each test, we checked whether the assumption required for that test was met, for example, we used the Ryan-Joiner normality test and Levene's test for equality of variances to examine the normality and equal variance of the data. We carried out a Wilcoxon signed-rank test to compare the initial and residual fiber lengths. We performed a Kruskal-Wallis test to analyze the effect of fiber content on the residual fiber lengths. We used a two-way analysis of variance (ANOVA) with a post-hoc Tukey HSD (Honestly Significant Difference) test to analyze the effect of the fiber aspect ratio (L/D) and the fiber content on tensile strength. We carried out a Kruskal-Wallis test with a post-hoc Dunn's test to analyze the effect of fiber content on the tensile modulus. Then, we also analyzed the effect of the fiber aspect ratio (L/D) on the tensile modulus using the Mann-Whitney test. To test whether the error of the estimated tensile strength and modulus values obtained with the rule of mixture model depends on the fiber content, we carried out a Kruskal-Wallis test. In the case of tensile strength, we also performed a posthoc Dunn's test. We carried out four separate Mann-Whitney tests to analyze the effect of fiber content and the fiber aspect ratio (L/D) on flexural strength and the flexural modulus. To analyze the effect of printing orientation on the tensile strength of 3D-printed materials, we carried out one-way analysis of variance (ANOVA) with a post-hoc Tukey HSD (Honestly Significant Difference) test. To analyze the effect of printing orientation on the tensile modulus of 3D-printed materials, we performed a Kruskal-Wallis test with a post-hoc Dunn's test. To compare the in-plane and interlayer tensile strength of the neat and fiber-reinforced materials, we performed a Wilcoxon signed-rank test and a paired T-test, respectively. Then, we carried out a Mann-Whitney test to determine whether there is a difference between the tensile strength anisotropy of neat and fiber-reinforced 3D-printed materials. For all analyses, a significance level of  $\alpha = 0.05$  was used.

15480569, 0, Downloaded from https://4spepublications.onlinelibrary.wiley.com/doi/10.1002/pc.29850 by Budapest University of Technology and Economics, Wiley Online Library on [21/08/2025]. See the Terms and Conditions (https://doi.org/10.1002/pc.29850 by Budapest University of Technology and Economics, Wiley Online Library on [21/08/2025]. See the Terms and Conditions (https://doi.org/10.1002/pc.29850 by Budapest University of Technology and Economics, Wiley Online Library on [21/08/2025]. See the Terms and Conditions (https://doi.org/10.1002/pc.29850 by Budapest University of Technology and Economics, Wiley Online Library on [21/08/2025]. See the Terms and Conditions (https://doi.org/10.1002/pc.29850 by Budapest University of Technology and Economics, Wiley Online Library on [21/08/2025]. See the Terms and Conditions (https://doi.org/10.1002/pc.29850 by Budapest University of Technology and Economics, Wiley Online Library on [21/08/2025]. See the Terms and Conditions (https://doi.org/10.1002/pc.29850 by Budapest University of Technology and Economics, Wiley Online Library on [21/08/2025]. See the Terms and Conditions (https://doi.org/10.1002/pc.29850 by Budapest University of Technology and Economics, Wiley Online Library on [21/08/2025]. See the Terms and Conditions (https://doi.org/10.1002/pc.29850 by Budapest University of Technology and Economics, Wiley Online Library on [21/08/2025]. See the Terms and Conditions (https://doi.org/10.1002/pc.29850 by Budapest University of Technology and Economics (https://doi.org/10.1002/pc.29850 by Budapest University of Technology (https://doi.org/10.1002/pc.29850 by Budapest University (https://doi.org/10.1002/pc.29850 by Budapest University (https://doi.org/10.1002/pc.29850 by Budapest University (https://doi.org/10.10

of use; OA articles are governed by the applicable Creative Commons

## 3 | FILAMENT PREPARATION AND FIBER BREAKAGE

The first step in 3D printing short fiber-reinforced composites is to prepare the fiber-reinforced filament. In general, the two main requirements aim to ensure a homogeneous distribution of fibers along the filament and to maintain a uniform filament diameter. Both are key to consistent print quality. Figure 2 summarizes the processing steps of filament preparation. Starting from a dry mixture of raw materials, the first step is to disperse the fibers in the thermoplastic matrix (compounding). This is mostly done by melting the polymer. The commonly used methods for melt mixing are internal mixing or twinscrew extrusion. In single-step processes, the filament and matrix are compounded to form a filament that can be used directly for 3D printing. Nasirov et al.66 prepared short carbon fiber-reinforced poly(lactic acid) (PLA) composites with a single extrusion step. The initial fiber length was 100 µm and the authors prepared composites with 5%, 7.5%, and 10% fiber volume fractions. Fiber distribution was uniform. Yu et al.<sup>67</sup> used chopped basalt fibers with an initial length of 3 mm and fabricated composite filaments with a co-rotating intermeshing twin-screw extruder. They used a special screw configuration optimized for filament production. It included a dispersive and a distributive mixing zone, and the fibers were fed in 6%-7% volume fraction through a second feeder. Lu et al.<sup>68</sup> presented a custom-made in-line mixing technique,

which was implemented straight on the 3D-printing head. With the method, it was possible to produce composites with up to 50% wt% fiber content. Carbon fibers with an initial length of 100–300  $\mu m$  and polyetheretherketone (PEEK) powder were used for the experiments. Overall, single-step methods are not widespread for filament production, as it is difficult to optimize the manufacturing parameters for standard processes in a single step.

In two-step processes, the first step is compounding (first melt mixing), which is followed by cutting. Then, the second step is filament preparation via extrusion (second melt mixing), during which the material is remelted. The purpose of the first melt mixing is to ensure a homogeneous distribution of fibers, and the second is to ensure a constant filament diameter. Therefore, in the first step, high-shear methods are preferred, which inevitably cause fragmentation of the fibers. Cutting may also slightly decrease the average fiber diameters.

In the case of two-step methods, internal mixers  $^{69-72}$  and twin-screw extruders  $^{73-76}$  are similarly common solutions for making composite compounds. After cutting the compounds, the filaments are almost always produced with a single-screw filament extruder. Tekinalp et al.  $^{71}$  used a plunger-type batch extruder to form the filaments with a diameter of 1.75 mm and reported a residual length of 200–380  $\mu$ m for 10–40 wt% carbon fiber composites. Abderrafai et al.  $^{73}$  also prepared the filament with the twin-screw extruder used for compounding, with the same processing parameters. In their case, the

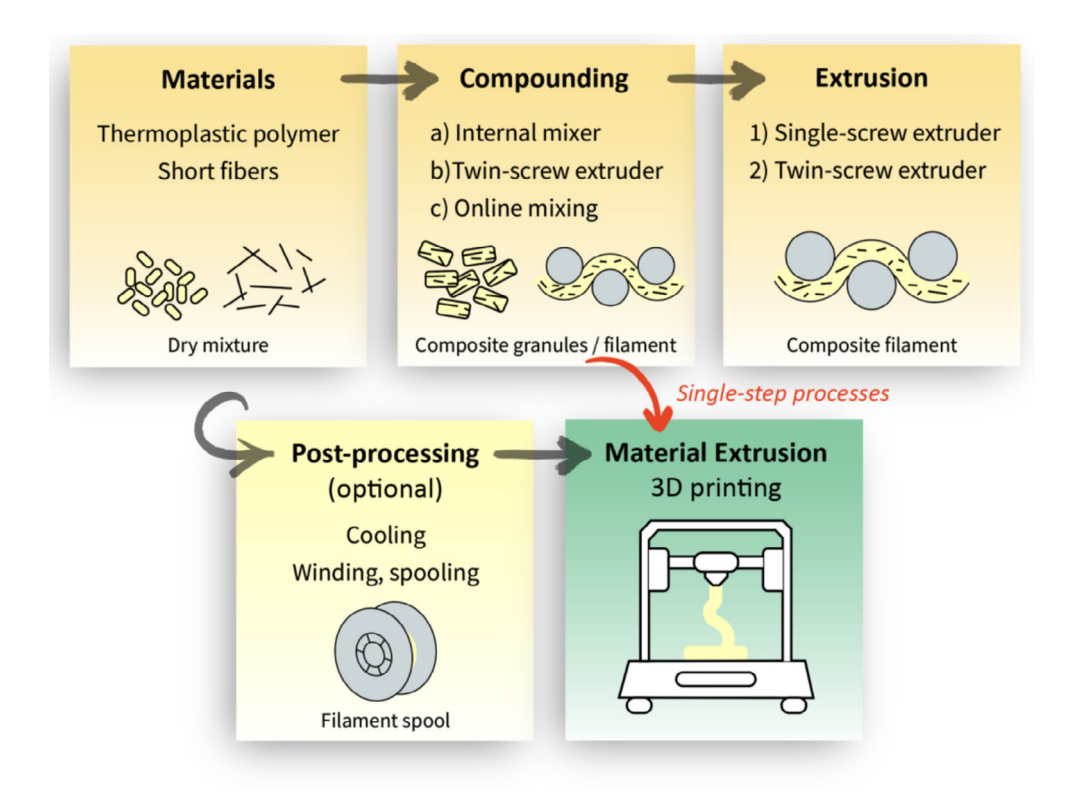


FIGURE 2 General manufacturing steps of filament production (single-step and two-step processes).

15480569, 0, Downloaded from https://4spepublications.onlinelibrary.wiley.com/doi/10.1002/pc.29850 by Budapest University of Technology and Economics, Wiley Online Library on [21/08/2025]. See the Terms

of use; OA articles are governed by the applicable Creative Commons

remaining length of the carbon fibers was 144 µm. The literature suggests that longer fibers can be produced with carefully chosen processing parameters. Sang et al. 70 achieved an average fiber length of 480 µm for basalt fiber-reinforced PLA composites using internal mixing followed by single-screw filament extrusion. Giani et al. 72 show that the use of recycled fibers does not necessarily lead to a higher degree of breakage. The authors reported the same processability for recycled carbon fibers as for virgin fibers, and achieved remaining lengths of 170 µm and 200 µm for 5 wt% and 10 wt%, respectively.

For obtained fiber lengths below 100 µm, it is typical that the initial length was also very small (below 300 µm). However, for values above 100 µm, there is no correlation with initial fiber length. Sang et al. 77 prepared basalt fiberreinforced PLA-PCL composites by twin-screw extrusion. The continuous basalt fiber tow was fed through the fiber feeding port by the rotation of the screw. Then, the authors prepared a composite filament with a desktop single-screw extruder. The two-step method resulted in a mean length of 225-230 µm. Despite the fact that the initial length was infinite, the remaining fiber length is only slightly longer than the average. Similarly, Tóth et al. 75

prepared basalt fiber-reinforced PLA composites with the two-step method (twin-screw extrusion compounding followed by single-screw extrusion) using fibers with an initial length of 10 mm. On average, the reduction in fiber length was 97%, the second highest of the data presented.

Figure 3A,B shows the fiber length (L) reduction for different materials and processing methods. For the analysis we made, 69 data points were taken from 17 research articles containing both single and two-step methods. The cumulative distribution function (CDF) of fiber length (F(L)) shows that the fiber length is reduced by at least one order of magnitude due to processing (Figure 3C). The CDF also shows that the residual fiber length does not depend on the initial length. The box plots show that the fibers have undergone significant fragmentation during processing (Figure 3D). This statement was also supported by a Wilcoxon signed-rank test (p < 0.001). The median  $(Q_2)$  of the initial mean length is 3200 µm, while the median of the remaining mean length is 196 µm. There is a large variance in the mean fiber length data (large interquartile range,  $IQR = 7750 \mu m$ ) for the initial length, while for the remaining length, there is a relatively narrow range (IOR =  $208 \mu m$ ). The maximum remaining length

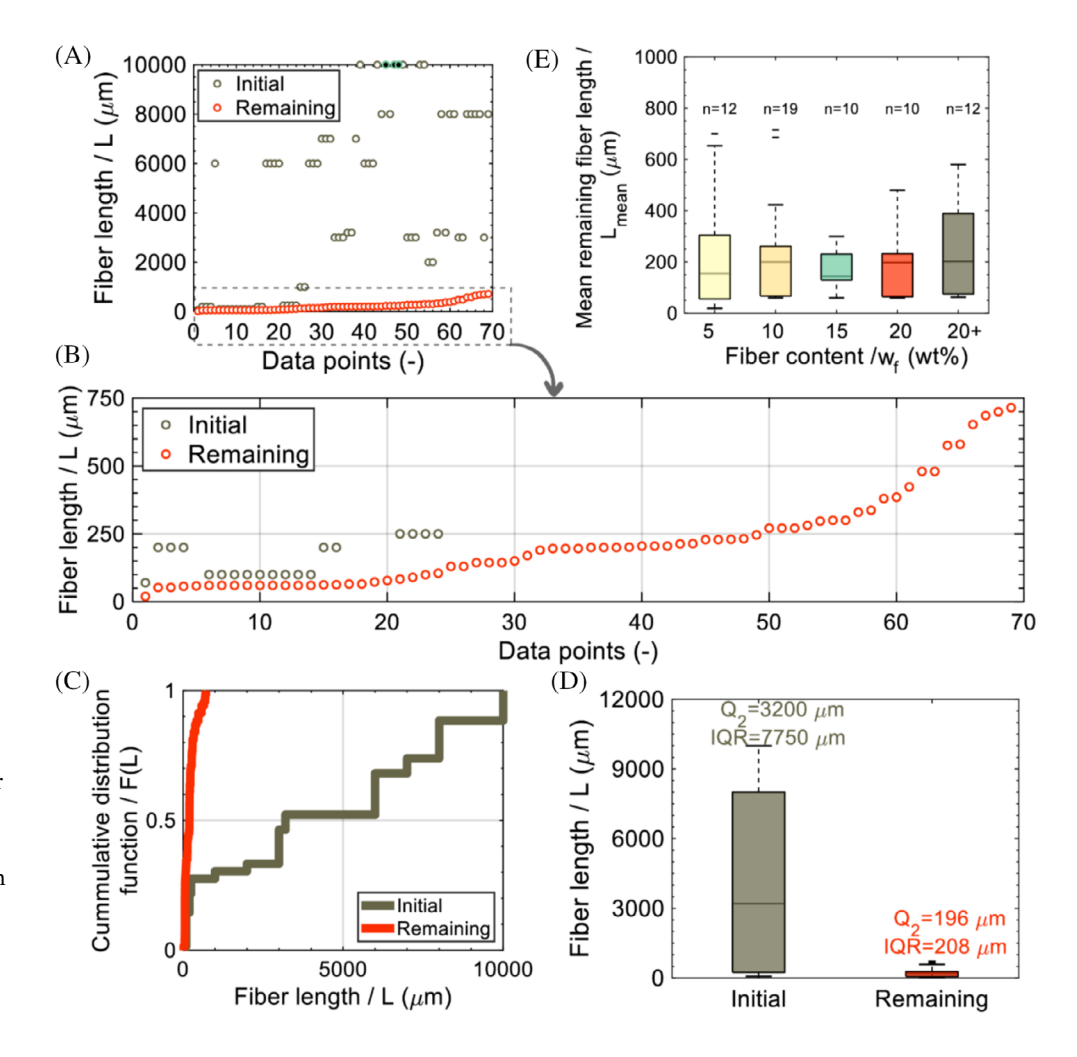


FIGURE 3 Analysis of fiber breakage during filament preparation. Initial and remaining fiber lengths sorted in ascending order of the remaining fiber length (A, B) (C) (D) (E). Data taken from.66-80

**TABLE 1** Modeling methods and the parameters used to estimate fiber breakage during twin-screw extrusion. 81–84

	0 0	
No.	Model	Parameters
Equation 1	$\frac{dL}{dt} = -k_f (L - L_{\infty})$	Remaining fiber length (L) Ultimate fiber length ( $L_{\infty}$ ) Kinetic constant ( $k_f$ ) Time (t)
Equation 2	$\frac{dL_{w}}{dt} = -K^{"}SME(L_{w} - L_{w\infty})$	Time-dependent weight average fiber length $(L_w)$ Time (t) Breaking rate constant (K) Specific mechanical energy (SME) Ultimate fiber length $(L_{w\infty})$
Equation 3	$P(Bu) = \frac{1 - \exp(Bu)}{1 - \exp(-1)} if Bu < 1$	Fiber breakage probability (P(Bu)) Buckling parameter (Bu)
Equation 4	$P_{y}(x) = \frac{\Gamma(2\alpha) \left(\frac{x}{y}\right)^{(\alpha-1)} \left(1 - \frac{x}{y}\right)^{(\alpha-1)}}{\Gamma^{2}(\alpha)}$	Gamma function (Γ)

was 700  $\mu$ m reported by Yu et al.,<sup>67</sup> who applied a single-step process. To examine the dependence of the remaining fiber length on fiber content, we divided the collected remaining mean fiber length (L<sub>mean</sub>) literature data into five groups based on fiber content (5,10,15,20 and 20+ wt%) (Figure 3E). Then, using the Kruskal-Wallis test, we found that the median values of each group were equal (p=0.946), that is, fiber content does not affect the remaining mean fiber length.

Fiber breakage in an extruder is primarily caused by shear and compressive forces exerted by the screw. Initially, the rate of breakage tends to be high but decreases over time as fibers shorten and become less susceptible to further damage. The rate of breakage also varies depending on fiber type; brittle fibers such as glass tend to break more easily than more ductile fibers. Thinner-diameter fibers are more flexible than thicker ones. Table 1 shows modeling methods used in the literature to estimate fiber breakage during twin-screw extrusion. Shon et al. <sup>81</sup> proposed a kinetic model to describe the deterioration of fiber length during compounding (Equation 1). Based on their study, Inceoglu et al. <sup>82</sup> introduced the specific mechanical energy (SME), an energetic parameter that accounts for the load on the fibers due to the viscosity of

the matrix material (Equation 2). Durin et al.<sup>83</sup> refined the model to consider the statistical nature of fiber breakage with the Weibull distribution function and verified the model with experimental data on glass fibers. They assumed that the fiber breakage takes place exclusively due to the buckling of the fibers induced by the flow, which causes huge local deformations. Equation 3 gives the probability of fiber breakage, where 'Bu' is the buckling parameter. The buckling parameter is the ratio of the stress induced by the flow on the fiber ( $\sigma_{\rm R}$ ) and the maximum stress before buckling  $(\sigma_m^e)$ , and is typically related to the critical load at which a fiber becomes unstable and undergoes buckling. Their model was then adapted by Malatyali et al.84 who described the fragmentation with a beta probability density function (Equation 4). Their model was verified for carbon fibers.

The type of thermoplastic polymer used as a matrix can also significantly influence fiber breakage due to differences in their rheological behavior. Amorphous polymers, such as ABS or polycarbonate, typically exhibit more gradual softening and higher melt viscosity, which can lead to higher shear stresses on the fibers in the extruder.85 This increased shear can contribute to fiber breakage. In contrast, semi-crystalline polymers, such as PLA or PEEK, exhibit a more pronounced melting transition and generally have a lower viscosity above their melting point, which can reduce the direct shear stress but can create compressive forces due to changes in flow behavior. 86 In addition, semi-crystalline polymers are more sensitive to repeated thermal cycling, potentially altering their viscosity and crystallization kinetics. Overall, in the case of FFF 3D printing, more research has focused on the effects of manufacturing parameters on fiber breakage, and the effects of the rheological properties of different matrix materials are less explored. This is a research gap that may be worth exploring further.

Fiber fragmentation also occurs in the nozzle during material extrusion. Yang et al.87 showed that a narrower nozzle and/or lower layer height induces greater shear, resulting in higher levels of fiber breakage. They showed that lower tensile strength and modulus are a consequence of higher rates of breakage. The authors found that more fiber breakage occurs during deposition. Hu et al.88 also showed that the deposition phase is damaging to the fibers due to the forces that are generated when the melt makes a 90° turn and is pressed against the print bed. Overall, the degree of fracturing in the nozzle is orders of magnitude lower than that during filament production. However, it has a detectable effect on the mechanical properties of the product, so the use of gentle printing parameters is recommended where higher mechanical strength is required.

**TABLE 2** Material properties, the properties of the 3D printing hardware, and the printing parameters that are deterministic at each level of a 3D-printed short fiber-reinforced composite structure.

Category	Bead	Lamina	Laminate
Hardware	<ul><li>Nozzle diameter</li><li>Nozzle length</li><li>Motor torque</li><li>Bed surface</li></ul>	Stability (vibration damping)	
Printing parameters	<ul><li>Nozzle temperature</li><li>Layer height</li><li>Bed temperature</li><li>Feed rate</li></ul>	<ul><li> Gap size</li><li> Degree of infill</li><li> Printing orientation</li><li> Infill pattern</li></ul>	<ul> <li>Ambient temperature</li> <li>Cooling rate</li> <li>Printing speed</li> <li>Part build orientation</li> <li>Layer order</li> <li>(Sublayer temperature)</li> </ul>
Material properties	<ul><li>Fiber content</li><li>Fiber-matrix adhesion</li><li>(Viscosity)</li></ul>	<ul><li>Thermal expansion coefficien</li><li>Heat transfer coefficient</li><li>Heat capacity</li></ul>	t

In summary, fiber breakage occurs during the filament manufacturing process, regardless of the nature of the process, and to a lesser extent in the nozzle as well during deposition. Our results, based on statistical analysis, show that the rate of fragmentation is independent of both the fiber content and the initial fiber length. Thus, reducing fiber breakage is a manufacturing optimization issue. An optimization solution could be to use a screw configuration with fewer shear elements and a lower compression ratio. Such a configuration can reduce the amount of shear on the fibers, but can also reduce the efficiency of the fiber distribution.

## 4 | MULTI-SCALE STRUCTURE

3D-printed parts are multiscale structures, where distinct levels can be identified based on the characteristic interfaces that define the macroscale properties. <sup>89</sup> With the use of this approach, three levels can be distinguished: bead, lamina, and laminate. Each level can be associated with key requirements, the fulfillment of which ensures

the quality of the printed product. Figure 4 shows a basic FFF 3D printing configuration. Table 2 shows the material properties, the properties of the 3D printing hardware, and the printing parameters that are deterministic at each stage. Figure 5 shows the multiscale structure and the main requirements and microstructural characteristics associated with each level. The parameters affecting the properties of these four levels are introduced in the following sub-chapters.

# 4.1 | The properties of the composite material in the nozzle

Before deposition, the composite melt is in the nozzle and the main requirement is printability. The characteristic interface is at the nozzle wall, where the shear forces impede the flow of the fluid and cause the orientation of the fibers. Printability means that the system pressure is equal to or greater than the pressure needed to overcome clogging. The mechanism of nozzle clogging is the packing and bridging of fibers in the internal cross-section of the

, Wiley Online Library on [21/08/2025]. See the Terms

of use; OA articles are governed by the applicable Creative Commons

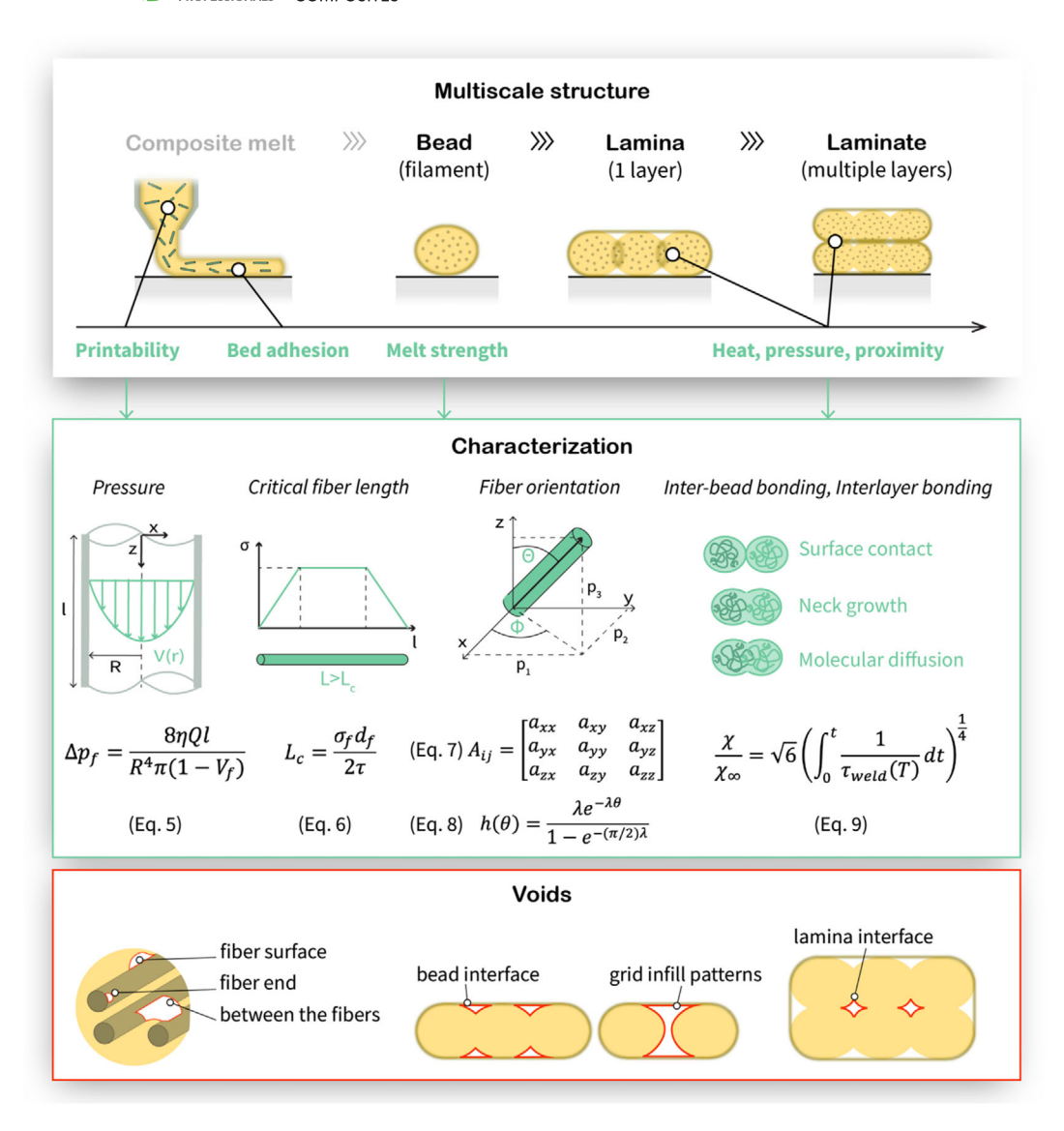


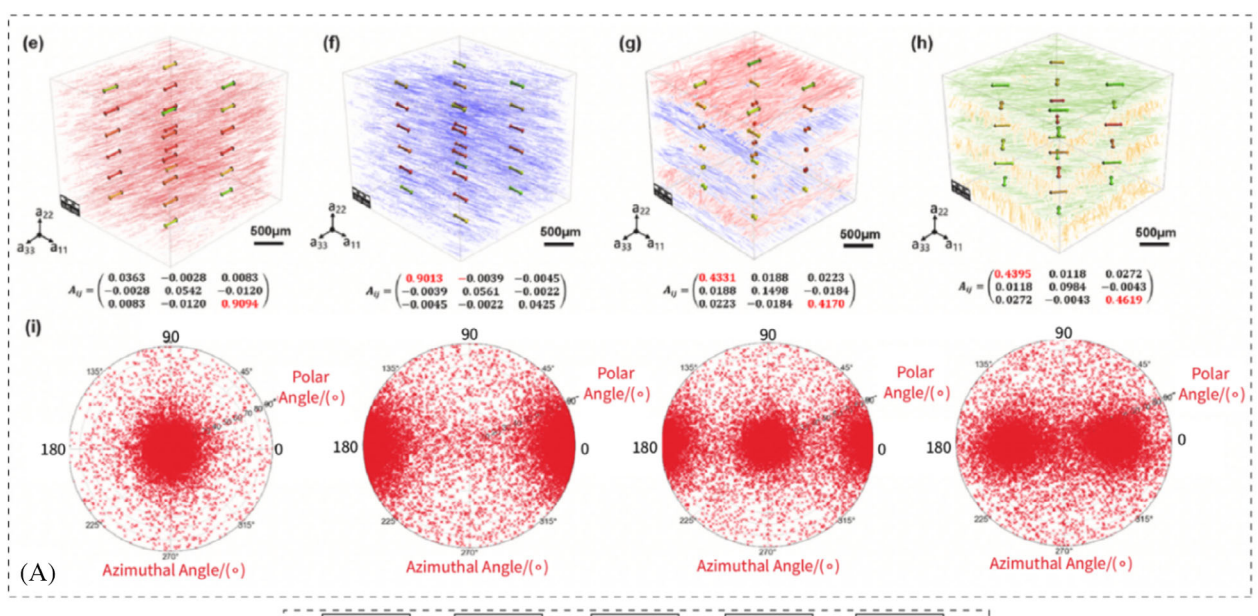
FIGURE 5 Multiscale structure of 3D-printed short fiber-reinforced composites and its main characteristic features.

nozzle. In a simplified approach, the pressure drop can be approximated based on the Hagen-Poiseuille relationship (Equation 5 in Figure 5), where  $\Delta p_f$  is the pressure drop (MPa), n is the viscosity as a function of shear rate at the temperature of the melt (Pas), Q is the volumetric flow rate (mm<sup>3</sup>/s), l is the length of the capillary (mm), R is the radius of the orifice (mm) and V<sub>f</sub> is the fiber volume fraction (-). However, to optimize the printing parameters, it is essential to understand the rheological behavior of the composite melt. 91,92 For example, it is recommended to perform capillary rheometer measurements and apply the Bagley correction to account for the inlet and outlet pressure drops, as well as the Rabinowitsch correction to calculate the true shear rate by taking into account the shear-thinning behavior of the polymer melt with a suitable power law exponent. 93,94 Zhang et al. 95 found that fiber clogging is dependent on fiber length. The

authors showed that clogging can be avoided with shorter fibers at higher fiber contents, as fiber bridging occurs less for shorter fibers.

# 4.2 | The properties and structure at bead level

When the composite melt is deposited on the print bed through the nozzle, it forms the first level of the 3D-printed structures, a single bead. One fundamental requirement is the proper adhesion to the print bed to ensure the geometrical accuracy of the product. Textured print beads, heated bed, and adhesive glues and sprays are often used to improve adhesion. The second requirement is sufficient melt strength to maintain layer height and bead geometry. The viscosity of the exiting melt is determined primarily by



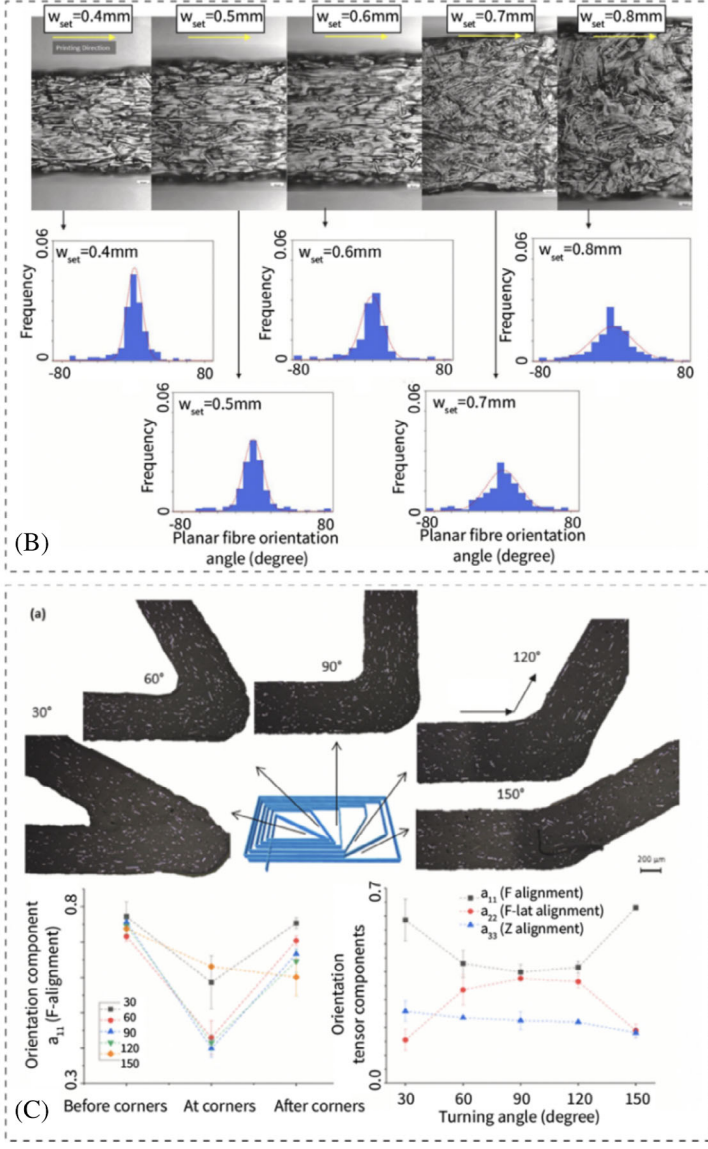


FIGURE 6 Legend on next page.

the temperature of the nozzle, and the rate of solidification is influenced by the ambient temperature and cooling rate. Das et al.<sup>97</sup> found that shear-thinning behavior is important to ensure successful material deposition and interdiffusion at later levels. The authors showed that in the case of carbon fiber–reinforced polyamide composites, higher zero shear viscosity ensured better geometrical stability of the bead.

At the bead level, the microstructural properties that influence the macroscale are fiber orientation, fiber-matrix adhesion, and the micro-voids. Fiber orientation is reported to be generally parallel to the printing direction. Yu et al. 98 presented a high degree of fiber alignment in the case of basalt fiber-reinforced PLA composites via micro-CT measurements (Figure 6A). Consul et al. 99 and Yan et al. 100 found that the nozzle diameter has the strongest effect on orientation, so narrower diameters cause a higher degree of fiber alignment (Figure 6B). This is to be expected, as the narrower the space into which the same flow of material is forced, the greater the shear stresses and the velocity gradient in the radial direction become, and the fibers will tend to arrange themselves in the direction of flow better. Shulga et al. 78 found that layer height has the same effect; that is, a smaller layer thickness causes a higher degree of orientation. Yan et al. 101 also showed that the increase in extrusion width and layer height led to a decrease in fiber alignment. At fiber intersections and corners, fiber orientation was lower (Figure 6C). Based on the results of carbon fiber-reinforced ABS and PLA, the authors showed that their findings are applicable for different matrix materials. Yang et al. 102 presented that the internal geometry of the nozzle also influences fiber orientation. The authors found fiber misalignment due to disruption in the flow field of the composite melt.

The fiber–matrix adhesion refers to the adhesive bonding strength between the fibers and the surrounding matrix. Strong adhesion ensures effective load transfer from the matrix to the fiber, and it determines critical fiber length. Critical fiber length is the minimum length a fiber must have to effectively bear the transferred stress. The Kelly-Tyson equation (Equation 6 in Figure 5) describes the critical length ( $L_c$ ) where the product of the strength of the single fibers ( $\sigma_f$ ) and the fiber diameter ( $d_f$ ) is divided by interfacial shear stress ( $\tau$ ). If the actual fiber length is higher than the critical fiber length, then the stress is properly transferred; thus, the fiber breaks in the composite. If the fibers' residual length is smaller

than the critical value, the fibers lose their connection with the matrix at a smaller load, that is, they get pulled out of the matrix, and the reinforcing effect becomes incomplete. In the case of 3D-printed composites, there are only a few research articles on the subject of fibermatrix adhesion. Yu et al.16 found that 3D-printed composites show distinctive mechanical behavior under different fiber-matrix adhesion conditions. In the case of strong adhesion, the authors reported an increase in tensile strength, and in toughness as well. In their study, the strong interfacial adhesion between the fibers and the matrix and the weak interfacial adhesion between the beads and the voids resulted in a tough behavior. Papon et al.<sup>17</sup> applied oxidation treatment on carbon fibers to increase bonding with a polylactic acid matrix. The better bonding reduced micro-voids at the fiber interface.

Without contact between the fiber and the matrix, micro-voids form along the fiber surface and at the fiber ends. Micro-voids can form near the fibers if the matrix does not fully impregnate the fibers, typically in the case of poor dispersion and high fiber content. Air entrapment voids can also form during compounding, and the presence of short fibers can increase the likelihood of air entrapment, especially in high viscosity thermoplastic melts. Fu et al. 103 reported an increase in micro-voids with increasing fiber content in carbon fiber-reinforced polyetheretherketone (PEEK) composites. They found that the micro-voids are one of the causes of the decrease in macro-scale tensile strength at higher fiber content. Shrinkage at the surface of the fibers may also initiate the formation of voids, as the fibers inhibit shrinkage of the surrounding matrix. At the fiber ends, voids form due to fiber pull-out during processing or due to fiber breakage. Yang et al. 102 found that at the bead level, most voids are formed when the material is extruded from the nozzle (in mid-air) as the polymer melt deforms and pulls away from the fibers (Figure 7A). In general, higher fiber content is generally associated with an increase in microvoids, as the number of fiber ends and the total surface area of fiber-matrix interfaces increases. Using a design of experiments, König et al. 104 analyzed the effects of parameter combinations on void formation. The printing temperature, speed, bead width, layer height, and the air gap were included. The authors identified combinations of printing parameters that can be used to achieve higher (and lower interfacial void content). Pei et al. 105 showed that printing speed also influenced void formation,

15480569, 0, Downloaded from https://4spepublications.onlinelibrary.wiley.com/doi/10.1002/pc.29850 by Budapest University of Technology and Economics, Wiley Online Library on [21/08/2025]. See the Terms and Conditions (https://doi.org/10.1002/pc.29850 by Budapest University of Technology and Economics, Wiley Online Library on [21/08/2025]. See the Terms and Conditions (https://doi.org/10.1002/pc.29850 by Budapest University of Technology and Economics, Wiley Online Library on [21/08/2025]. See the Terms and Conditions (https://doi.org/10.1002/pc.29850 by Budapest University of Technology and Economics, Wiley Online Library on [21/08/2025].

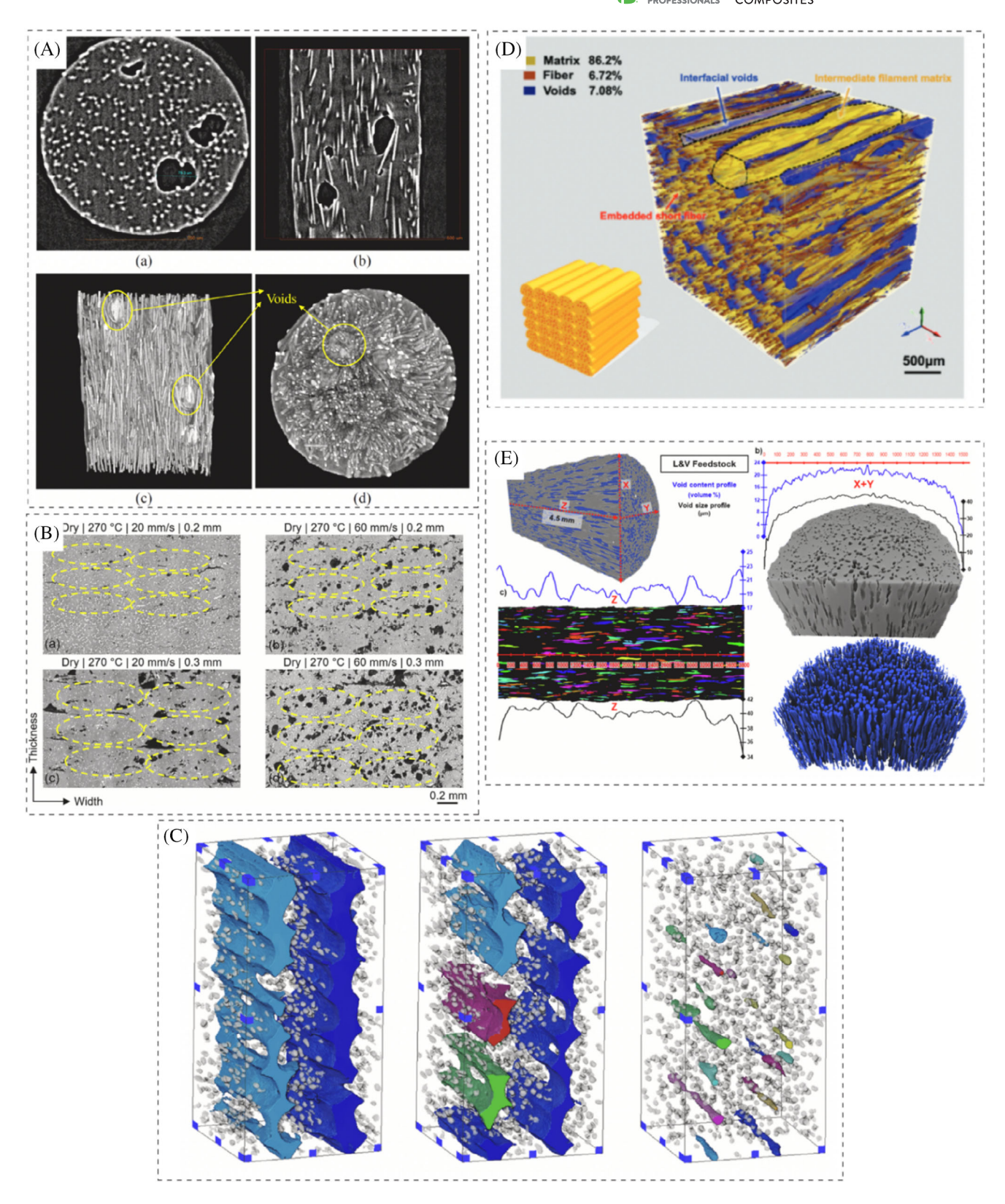


FIGURE 7 Different types of void formations in short fiber–reinforced 3D-printed composites (A) Voids form in mid-air as the polymer melt deforms and pulls away from the fibers<sup>102</sup> (B) Lower layer height reduces the number of voids within the bead<sup>105</sup> (C) Increasing the extrusion rate decreases the voids between the beads: Effects of extrusion multiplier of 0.9, 1, and 1.1 (left to right) on the void content<sup>106</sup> (D) 3D microtomography image showing voids between the beads with color segmentation,<sup>69</sup> (E) 3D visualization of void distribution in a bead showing void content and size profiles.<sup>107</sup>

as samples printed at lower speeds had fewer voids. Moreover, the authors found that applying a lower layer height reduced the number of voids within the bead due to the higher applied pressure (Figure 7B). Tikhani et al. 106 investigated the effects of printing temperature, extrusion rate, and fiber content on void content in the case of carbon fiber-reinforced PC composites. The authors showed that increasing the extrusion rate decreases the porosity between the beads (Figure 7C). However, porosity in the beads was not significantly affected, as the authors attributed its extent to the moisture content of the matrix. Sommacal et al. 107 presented 3D visualization of void distribution along a 3Dprinted bead. They found that the average void content is higher toward the center, and its distribution is more homogeneous along the z direction (Figure 7E).

### 4.3 The properties and structure of the lamina

The second level is when the beads are extruded next to each other to form a lamina. The pattern and the number of beads in a lamina are highly customizable. The new interface is at the connection of the beads where the polymer matrix bonds. Bond strength influences macroscale properties. The requirement for bonding is the proximity of beads and sufficient heat to melt the polymer. The pattern and the number of beads in a lamina are customizable. Based on the methodology proposed by Bellehumeur et al. 108 and adapted by others, 109,110 the bonding mechanism is best described as polymer sintering. The bond develops from surface contact to neck growth and molecular diffusion with chain randomization. The viscosity of the polymer melt should be low enough for complete coalescence, because partial bonding leads to the formation of voids. 19,111 At the surface contact stage, the deposited material wets and reheats the previous beads. Sintering is driven by surface tension, and it is affected by viscosity and the mobility of polymeric chains; therefore, it depends on temperature besides material properties. The temperature profile is a function of several manufacturing parameters, of which nozzle temperature, ambient temperature, and the cooling rate are reported to be the dominant features for bonding quality. Besides these input parameters, the temperature profile is also a function of heat transfer mechanisms. Bond formation depends on the conductive heat transfer between the beads, as the previous beads have already started to solidify after deposition. As the structure solidifies, internal stresses form due to constraints caused by the previous bonds and shrinking; therefore, bond strength is greatly affected by the cooling rate as well. Predictive methods for bond strength are studied extensively to this day, but

models that incorporate fibers as well are scarce. As the thermal conductivity of different types of fibers varies, it is expected that the bond formation of different fiber-filled composites will vary as well. The effects of fiber content should also be considered.

## 4.4 | The properties and structure of the laminate

At the third level, laminas are stacked on each other, thus forming a laminate. The new interfaces are created between the laminas. Lower layers must withstand the compression stress caused by the combined weight of the top layers. 90 In the case of fiber-reinforced materials. this is not a crucial issue. As shown in Figure 5, the beads placed side by side are basically circular in cross-section, flattening out slightly as they are laid down. Depending on the gap size used between the beads, the lamina surface is not expected to be flat. Thus, characteristic voids will appear in the laminate between the stacked laminas. The geometry and the number of voids in the laminate also depend on the printing orientation and the layering of the single laminas. Kubota et al. 112 found that larger gaps are generated between the beads when a layer order of ±45° is applied. In the case of short fiber-reinforced composites, Tekinalp et al.<sup>71</sup> reported that in the laminate, void formation is dependent on fiber content. With more fibers, the number of micro-voids increased while interlayer voids decreased. This was also confirmed by Yu et al.<sup>69</sup> via X-ray microscopy (Figure 7D).

For molecular bonding, heat and pressure are required. Coogan and Kazmer<sup>113</sup> described interlayer diffusion with Equation 9 (in Figure 5). The quality of the interlayer bonding greatly influences the macroscale characteristics, yet the effect of fibers on the bonding process is a less researched area. It can be expected that the fiber content influences the bonding process, as more fibers at the layer interface can hinder polymer diffusion. The rate of interlayer diffusion is strongly influenced by the amount of heat and the time of thermal exposure. Different types of fibers have different thermal properties, and the heat transfer coefficient between the fiber and the matrix also varies. Therefore, the effects of fibers on the interlayer bonding should be incorporated into future studies.

# MICROSTRUCTURE AND **MECHANICAL PROPERTIES**

The multi-level structure of the printed parts that was introduced in the previous chapter leads to unique structural and mechanical characteristics. The development of

15480569, 0, Downloaded from https://4spepublications.onlinelibrary.wiley.com/doi/10.1002/pc.29850 by Budapest University of Technology and Economics, Wiley Online Library on [21/08/2025]. See the Terms

of use; OA articles are governed by the applicable Creative Commons

macro-level mechanical properties is governed by the complex effects of manufacturing parameters and material properties. We carried out a statistical analysis to reveal the effects of the microstructure on mechanical properties. The analysis seeks answers for the current limitations of short fiber-reinforced 3D-printed composites. Fiber content, fiber aspect ratio, and fiber orientation were considered in the analysis of tensile and flexural strength and modulus. We also investigated the anisotropic nature of 3D-printed composites by analyzing the effect of different printing directions in-plane and by examining the differences between in-plane and interlayer properties.

# Effect of fiber aspect ratio and fiber content on tensile properties

The fiber aspect ratio (L/D, i.e., length over diameter) was used in analyzing the effect of fiber geometry. In general, fibers are usually considered to have an aspect ratio of greater than 10, while particles or fillers typically have aspect ratios below 10. A high aspect ratio typically means that the fiber is long and thin, which, in the case of good fiber-matrix adhesion, is expected to significantly enhance the mechanical properties of the composite.

The matrix material of the composites collected from the literature varies. The fiber types are carbon (43), basalt (31), and glass (8), and the matrix materials are PLA (47),

PEEK (13), PA (12), ABS (7), PP (3), PETG (2). Therefore, to compare the results measured on different materials, we calculated relative tensile strength ( $\sigma_{t,rel} = 100$  $(\sigma_{t,comp}/\sigma_{t,neat}))$  and relative tensile modulus  $(E_{t,rel} = 100)$ (E<sub>t.comp</sub>/E<sub>t.neat</sub>)) as the ratio of the tensile strength/ modulus of the composite to that of the neat material, expressed as a percentage. Relative strength and relative modulus (Figure 8A,B) show the percentage increase/ decrease in tensile strength and modulus when fibers are added. We collected 82 and 73 data points for tensile strength and Young's modulus, respectively. In Figure 8, the relative tensile properties are plotted as a function of fiber content (1–50 wt%) and fiber length (19–715  $\mu$ m).

The tensile strength data were analyzed with respect to fiber content (w<sub>f</sub>) and fiber aspect ratio (L/D). First, based on fiber content, the data were divided into five groups (5, 10, 15, 20, 20+ wt%); after that, each group was subdivided according to the L/D values (L/D < 10, L/D > 10) (Figure 8C). Then, we carried out a two-way ANOVA.

The analysis showed that the fiber aspect ratio (L/D) has no significant effect on tensile strength (p = 0.782). This is unexpected, as a close relationship between strength and fiber length is expected when there is good adhesion between the fibers and the matrix. Longer fibers are likely to have a greater strength-enhancing effect. Therefore, the lack of strengthening effect suggests that fiber-matrix adhesion was insufficient in most studies. Regarding fiber content, considering only the mean values, an increase in the fiber content leads to a trend-wise

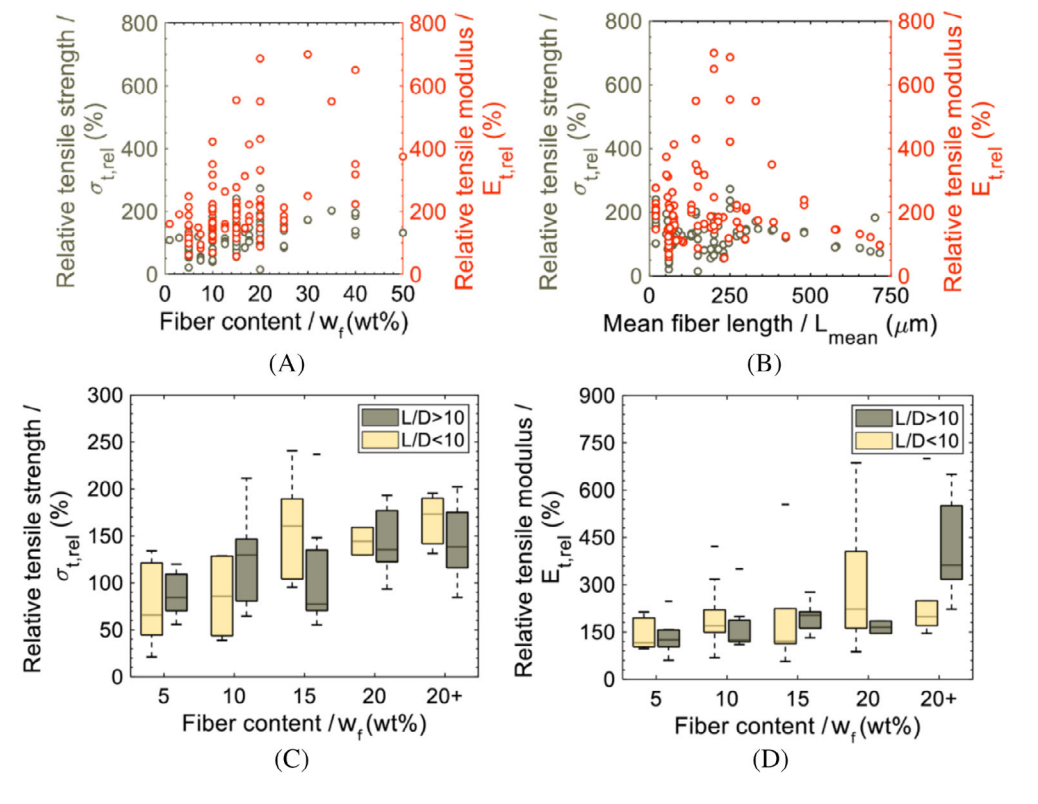


FIGURE 8 Tensile properties (A) relative tensile strength and relative tensile modulus (Young's modulus) as a function of fiber content (w<sub>f</sub>), (B) relative tensile strength and modulus as a function of mean fiber length (Lmean), (C) comparison of tensile strength data based on the L/D ratio, (D) comparison of tensile modulus data based on the L/D ratio.66-77,79,80,114-117

15480569, 0, Downloaded from https://4spepublications

onlinelibrary.wiley.com/doi/10.1002/pc.29850 by Budapest University of Technology and Economics

, Wiley Online Library on [21/08/2025]. See the Terms

on Wiley Online Library for rules of use; OA articles are governed by the applicable Creative Commons

**TABLE 3** Results of the statistical analysis for relative tensile strength and relative tensile modulus. Cases with the same letter in the Grouping column of the tables are considered statistically identical.

	Relative tensile strength				Relative tensile modulus	
w <sub>f</sub> (wt%)	Number of data points	Mean of relative tensile strength (%)	Group	ing	Number of data points	Median of relative tensile modulus (%)
5	14	83	-	В	12	124
10	23	105	A	В	18	167
15	22	130	A	-	18	195
20	11	148	A	-	13	215
20+	12	155	A	-	12	283

increase in strength (Table 3). The maximum increase in tensile strength achieved by fiber reinforcement was 2.7 times. Note that in the majority of the  $w_f = 5$  wt% cases, the addition of fibers reduced tensile strength (Figure 8A). With a fiber content of 20+ wt%, the mean increase in tensile strength is 55% (Table 3). When the variance of the data is taken into account, we can say that a fiber content of 15 wt% and above had a significantly stronger effect than 5 wt% and below (Table 3). However, based on a one-way ANOVA test, no significant difference can be found between the 10, 15, 20, and 20+ wt% fiber content groups (p=0.109).

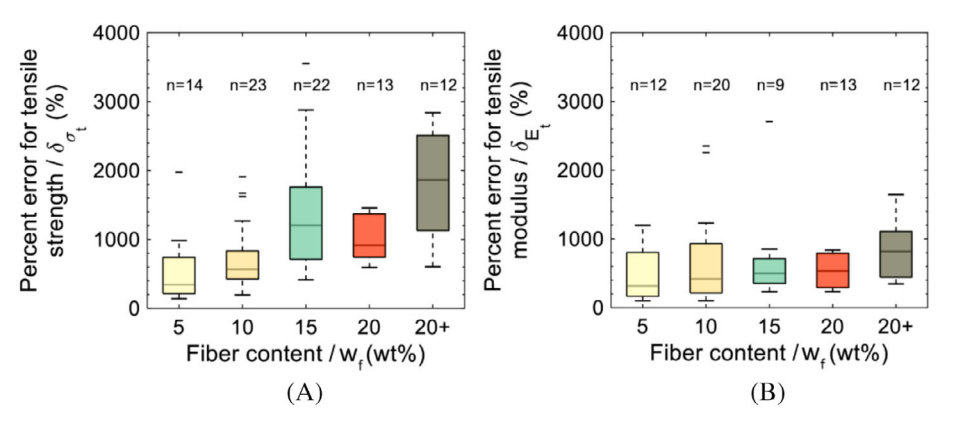
In the case of the tensile modulus, the data were divided into five groups based on fiber content (5, 10, 15, 20, 20+ wt%) (Figure 8D). Considering the median values only, we can say that an increase in fiber content leads to a trend-wise increase in the tensile modulus (Table 3). In many cases, the addition of fibers resulted in more than a twofold increase in tensile modulus, but in some cases five-to sevenfold increases were achieved. In contrast to tensile strength, tensile modulus can be increased in most cases with as little as 5 wt% fiber content. We performed a Kruskal-Wallis test with a post-hoc Dunn's test to show the effect of fiber content on the relative tensile modulus (Table 4). Pairwise comparisons of each group showed a significant difference only between 5 and 20+ wt% fiber content. 20+ wt% had a significantly stronger effect on tensile modulus than 5 wt% and below (p = 0.003). However, the analysis also showed no significant difference between the relative tensile modulus of composites with 5, 10, 15, and 20 wt% fiber contents. Higher modulus at higher fiber content is expected, as fibers generally have a modulus at least an order of magnitude larger than the matrix, so a larger fraction will result in an increase. The embedded fibers can also restrict the deformation of the matrix under load at room temperature, making the composite stiffer. The increase between low and high fiber contents suggests that the

**TABLE 4** Post-hoc pairwise comparisons of the relative tensile modulus of groups with different fiber contents using Dunn's Test  $(Q_{crit} = 2.7996)$ .

Compared groups	Q value	Decision on null hypothesis
20+ — 5	3.6849	Reject H <sub>0</sub>
20+ — 10	2.7965	Fail to reject H <sub>0</sub>
20+ — 15	No comparison made	Accept H <sub>0</sub>
20+ — 20	No comparison made	Accept H <sub>0</sub>
20 — 5	2.5533	Fail to reject H <sub>0</sub>
20 — 10	No comparison made	Accept H <sub>0</sub>
20 — 15	No comparison made	Accept H <sub>0</sub>
15 — 5	1.7390	Fail to reject H <sub>0</sub>

effect of fiber content can be described by models based on the rule of mixtures. However, the statistical analysis showed that modulus does not correlate with fiber content. Therefore, modeling likely requires the application of correction factors to express the increment rate. We analyzed the effect of the fiber aspect ratio (L/D) on the tensile modulus using the Mann-Whitney test. The relative tensile modulus data was divided into two groups based on the L/D ratio (L/D < 10 and L/D > 10). We found that the L/D ratio does not influence the relative tensile modulus (p = 0.868). In the analysis of the relationship between the tensile strength data and the L/D ratio, we found that the parameters are independent, so a weak fiber-matrix relationship can be assumed. For the tensile modulus, there is no major impact of the fibermatrix relationship. The effect of the fiber-matrix relationship is most pronounced during failure and thus affects the strength of the composite.

The data points show that an average increase of  $2.22 \pm 1.41$  times in tensile modulus can be achieved by using short fiber reinforcement. In the case of tensile strength, only



a moderate average increase of  $1.25\pm0.5$  times can be expected. The statistical analysis results suggest that increasing fiber content cannot guarantee an improvement in tensile properties.

Analysis was also carried out by comparing the theoretically achievable tensile strength and modulus estimated from the literature data using the simple rule of mixtures (RoM). The estimates given by the RoM take into account the fiber type and the fiber volume or weight ratio. However, they ignore any structural characteristics and defects that may occur in the composite. The comparison thus shows the effect of microstructural characteristics of short fiber composites on mechanical properties. The modeling of microstructural features such as fiber length distribution, fiber orientation, or void content is the subject of later chapters.

We calculated the percent error  $(\delta)$  between the RoMestimated and the measured values for tensile strength and Young's modulus as  $\delta_{\sigma}=(|\sigma_{t,RoM}-\sigma_t|/\sigma_t)^*100$  and  $\delta_E=(|E_{t,RoM}-E_t|/E_t)^*100$ , respectively. Figure 9A,B shows the percent error for tensile strength and modulus as a function of fiber content, respectively. In both cases, even the smallest median value of percent error was more than 300% (at 5 wt% fiber content). The RoM gives the theoretical tensile strength and modulus for a given fiber content, assuming continuous fibers. The magnitude of the deviation demonstrates that structural features other than ideal, such as shorter fibers, non-unidirectional fiber orientation, and voids, need to be taken into account to a large extent in predictive calculations.

Using a Kruskal-Wallis test with a post-hoc Dunn's test we showed that there is no correlation between percentage errors for tensile strength and fiber content (Table 5). In the case of Young's modulus, a Kruskal-Wallis test also showed that the percent error does not depend on fiber content (p=0.218). However, percent errors for tensile strength are significantly larger at 20+ wt% than at 5 wt% cases (p<0.001), and the median values show a trend increase as a function of fiber content. A smaller increase can also be observed for the modulus medians as a

**TABLE 5** Post-hoc pairwise comparisons of the relative percent error for tensile strength of groups with different fiber contents using Dunn's Test ( $Q_{crit} = 2.7996$ ).

Compared		Decision on
groups	Q value	null hypothesis
20+ — 5	4.5902	Reject H <sub>0</sub>
20+ — 10	4.0677	Reject H <sub>0</sub>
20+ — 20	1.6648	Fail to reject $H_0$
20+ — 15	No comparison made	Accept H <sub>0</sub>
15 — 5	3.7702	Reject H <sub>0</sub>
15 — 10	3.1243	Reject H <sub>0</sub>
15 — 20	0.4278	Fail to reject $H_0$
20 — 5	2.9580	Reject H <sub>0</sub>
20 — 10	2.2539	Fail to reject $H_0$
10 — 5	1.0539	Fail to reject H <sub>0</sub>

function of fiber content. This suggests that the degree of deviation from the theoretical mechanical properties increases with higher fiber content. The dominant microstructural features, fiber length and orientation, are not discrete values but follow a distribution. As the ratio of fibers increases, the proportion of fibers in non-ideal conditions and the number of defects in the composite also increases. As a result, the macro-scale properties of the composite become less and less comparable to the theoretically achievable properties, and the accuracy of prediction methods is expected to decrease for higher fiber contents.

Lastly, in the case of Young's modulus, the percent errors at 15 wt% and higher fiber contents are significantly smaller than those for tensile strength. The Young's modulus is calculated from the initial, linear phase of the stress–strain curve. This region typically represents elastic deformation, where fiber-reinforced composites behave in a more predictable, linear manner. In contrast, tensile strength is the result of failure processes that often involve complex damage mechanisms beyond

15480569, 0, Downloaded from https://4spepublications.onlinelibrary.wiley.com/doi/10.1002/pc.29850 by Budapest University of Technology and Economics

, Wiley Online Library on [21/08/2025]. See the Terms

of use; OA articles are governed by the applicable Creative Commons

LWILEY\_spe

the elastic region. This includes fiber breakage, fiber pullout, matrix cracking, and debonding at the fiber-matrix interface. Therefore, the tensile strength is expected to deviate more from the theoretical value than the Young's modulus. This also means that analytical models are expected to be less precise when used for tensile strength, as many analytical models assume idealized conditions such as perfect fiber-matrix adhesion or uniform fiber length.

# The effect of the fiber aspect ratio and fiber content on flexural properties

In Figure 10A,B the 22 data points for relative flexural strength and 16 points for flexural modulus are plotted as a function of fiber content (1-50 wt%) and fiber length (52-271 µm). The material of the composites collected from the literature varies. The fiber types are carbon (15), basalt (4) and glass (3), the matrix materials are PEEK (16), ABS (4) and PLA (2). To analyze the flexural properties measured on different materials, we calculated relative flexural strength ( $\sigma_{f,rel} = 100 \ (\sigma_{f,comp}/\sigma_{f,neat})$ ) and relative flexural modulus ( $E_{f,rel} = 100 (E_{f,comp}/E_{f,neat})$ ) as the ratio of that of the composite to that of the neat material expressed as a percentage.

The data were analyzed by fiber content (10 wt% or lower, and above) and fiber aspect ratio (L/D < 10, L/D > 10) (Figure 10C,D). The median values of relative flexural strength and relative flexural modulus for each

group are shown in Table 6. Using two separate Mann-Whitney tests, we showed that fiber content has no significant effect either on flexural strength (p = 0.891) or modulus (p = 0.143). However, the fiber aspect ratio has a significant effect on both. Two separate Mann-Whitney tests showed that L/D < 10 resulted in a significantly higher increase in flexural strength (p = 0.005) and modulus (p = 0.008) than L/D > 10. This is the opposite of what one would expect. With proper fiber-matrix adhesion, longer fibers have a larger surface area; therefore, they can provide better load distribution. Thus, longer fibers are expected to enhance both properties. Consistent with the analysis of tensile properties, the results suggest that fiber-matrix adhesion was insufficient in the presented studies. The maximum increase in flexural strength and modulus achieved by the addition of short fibers is 3.5 and 5.7 times, respectively. Overall, fiber reinforcement is expected to significantly increase the flexural modulus by an average of  $2.69 \pm 1.35$  times, but only a moderate increase in strength of  $1.34 \pm 0.69$  can be expected.

#### 5.3 Analysis of anisotropy

### In-plane direction-dependent tensile 5.3.1 properties

3D-printed structures are anisotropic, meaning there can be a large difference between the in-plane (x, y) mechanical properties and those perpendicular to it (in z direction)

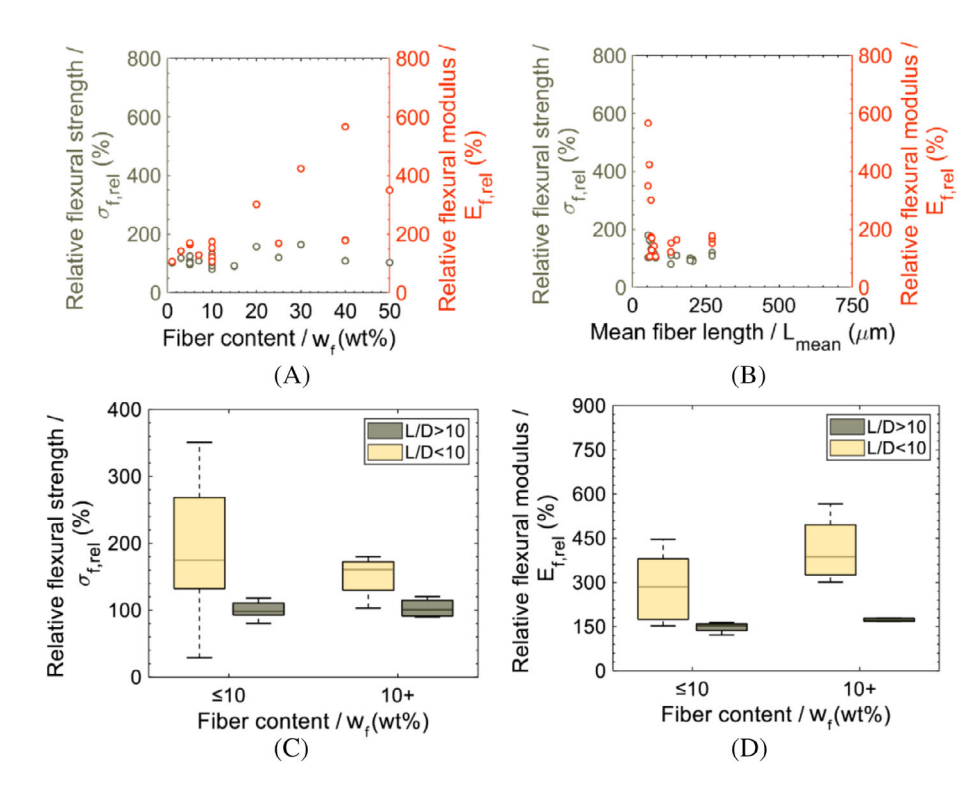


FIGURE 10 Flexural properties (A) relative flexural strength and modulus as a function of fiber content (w<sub>f</sub>), (B) relative flexural strength and modulus as a function of mean fiber length (L<sub>mean</sub>), (C) comparison of flexural strength data based on the L/D ratio, (D) comparison of flexural modulus data based on the L/D ratio. 68,70,74,76,79,115,118-121

**TABLE 6** Median flexural strength and modulus values for the different groups.

	Relative flexural strength		Relative flexural modulus		
Group	Number of data points	Median value (%)	Number of data points	Median value (%)	
$w_f \le 10 \text{ wt}\%$	14	111	10	170	
$w_f > 10 \text{ wt}\%$	8	115	6	326	
L/D < 10	10	161	10	352	
L/D > 10	12	98	6	159	

FIGURE 11 Tensile properties as a function of printing orientation
(A) Interpretation of printing orientation in a coordinate system, (B) tensile strength of fiber-reinforced materials, (C) tensile modulus of fiber-reinforced materials, (D) relative tensile strength, (E) relative tensile modulus.

66,6971,73,74,77,9,114,116,117,120,126

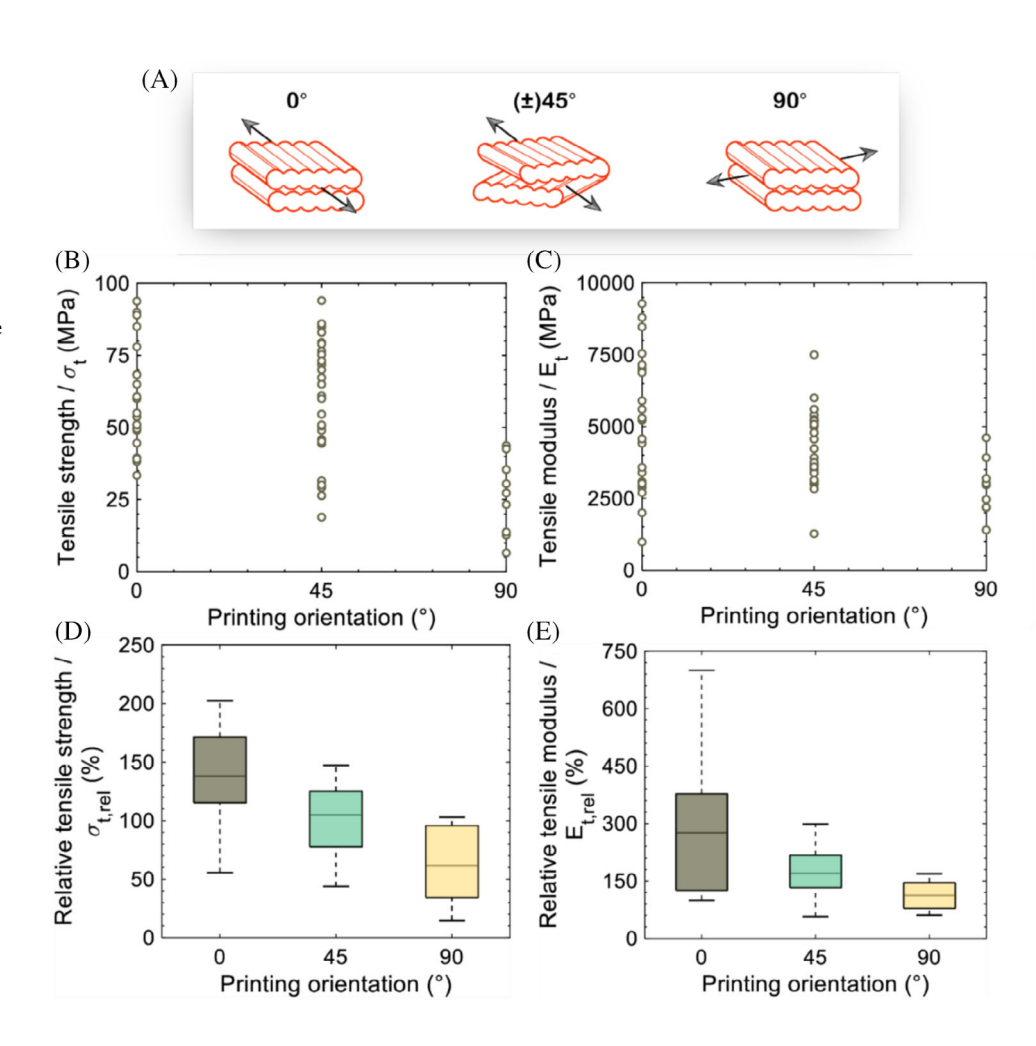


(Figure 11A). Numerous studies have investigated interlayer bonding in the case of neat polymers, and it has been shown that fillers and reinforcements affect the anisotropy of mechanical, <sup>122,123</sup> functional <sup>124</sup> and tribological <sup>125</sup> properties.

Figure 11B-E shows the effect of printing orientation on tensile properties (67 and 59 data points for tensile strength and modulus, respectively). Since 3D printing has been shown to align the fibers mostly in the direction of the toolpath, our study indirectly reveals the effect of fiber orientation. The main directions are distinguished in respect to the load direction: parallel to it (0°), perpendicular to it (90°), and at an angle of 45°. (Samples

printed at 45° often have alternating layering, so in some instances the orientation in the laminate is  $\pm 45^\circ$ ). To compare the results measured on different materials, we calculated relative tensile strength ( $\sigma_{t,rel}=100~(\sigma_{t,comp}/\sigma_{t,neat})$ ) and modulus ( $E_{t,rel}=100~(E_{t,comp}/E_{t,neat})$ ) as the ratio of the tensile strength/modulus of the composite to that of the neat polymer expressed in percentage.

To statistically analyze the effect of printing orientation on the tensile strength of 3D-printed materials, we performed a one-way ANOVA with a post-hoc Tukey HSD test (Table 7). The results show that relative tensile strength in the  $0^{\circ}$  printing direction is significantly higher than that in the  $45^{\circ}$  printing direction. Also, in

15480569, 0, Downloaded from https://4spepublications

onlinelibrary wiley com/doi/10.1002/pc.29850 by Budapest University of Technology and Economics, Wiley Online Library on [21/08/2025]. See the Terms and Conditions (https://onlinelibrary.wiley.

.com/terms-and-conditions) on Wiley Online Library for rules of use; OA articles are governed by the applicable Creative Commons

**TABLE 7** Results of the statistical analysis for relative tensile strength and relative tensile modulus values. Cases with the same letter in the Grouping column of the tables are considered statistically identical.

Printing orientation (°)	Number of data points	Mean value of relative tensile strength (%)	Grou	aping		Number of data points	Median value of relative tensile modulus (%)
0	25	138	A	-	-	25	276
45	33	101	-	В	-	25	170
90	9	63	_	-	C	9	112

the 45° direction, strength is significantly higher than in the 90° direction (p < 0.001). This means that printing orientation is statistically proven to have a trend-like effect on the tensile strength of 3D-printed short fiber-reinforced composites. Overall, the data points show that the strength enhancement effect with the addition of fibers is on average  $1.38 \pm 0.42$  times when the orientation is 0°. This is  $1.01 \pm 0.3$  times when the orientation is 45°, so it is practically unchanged. Lastly, strength decreases by  $0.63 \pm 0.34$  times due to the addition of fibers when the orientation is 90°. The maximum increase in tensile strength was 3% for the 90° orientation. This is in agreement with the phenomenon established in the literature that fibers are largely oriented in the printing direction, as fibers parallel to the load perform the most efficient reinforcement.

For tensile modulus, the median values show that the larger the deviation of the printing angle from 0°, the smaller the increment (Table 7). To statistically analyze the data points, we performed a Kruskal-Wallis test with a post-hoc Dunn's test (Table 8). A pairwise comparison of each group shows that there is a significant difference between the relative tensile modulus of the 0° and 90° orientations (p < 0.001). There is no difference between  $0^{\circ}$  and  $45^{\circ}$  and between  $45^{\circ}$  and  $90^{\circ}$ . Based on the data, the addition of fibers is expected to increase the tensile modulus by an average of  $3.00 \pm 1.75$  and  $1.72 \pm 0.56$  times in the  $0^{\circ}$  and  $45^{\circ}$  printing directions, respectively. In the  $90^{\circ}$ printing direction, the tensile modulus remains approximately unchanged  $(1.11 \pm 0.38 \text{ times increase})$ . However, the directional dependence of the tensile modulus is statistically confirmed only between the extremes ( $0^{\circ}$  and  $90^{\circ}$ ), so it is not sensitive to small changes in fiber orientation on average.

In the analysis, unidirectional (0°, 90°, 45°) and occasionally bidirectional ( $\pm 45^{\circ}$ ) composites were investigated. However, 3D printing also allows for additional layering and quasi-isotropic orientations. Távara et al. <sup>127</sup> investigated the tensile properties of bidirectional carbon fiber–reinforced PA composites. The authors found that better properties can be achieved with a layer order of 0°/90° than with  $\pm 45^{\circ}$ . However, the latter showed more favorable fracture properties. According to the literature, print orientation has the most effect on tensile properties;

**TABLE 8** Post-hoc pairwise comparisons of the relative tensile modulus of groups with different printing orientations using Dunn's Test ( $Q_{crit} = 2.3877$ ).

Compared		Decision on
groups	Q value	null hypothesis
0 — 90	3.7679	Reject H <sub>0</sub>
0 — 45	2.3138	Fail to reject H <sub>0</sub>
45 — 90	2.0843	Fail to reject $H_0$

for other types of loads, it is less dominant or its effect is less obvious. Iyer and Keles<sup>128</sup> showed that flexural properties are less dependent on the printing orientation.

# 5.3.2 | Interlayer tensile properties

3D-printed composites with short fiber reinforcement exhibit higher tensile strength due to the alignment of the fibers along the printing direction. However, this directional alignment results in reduced strength when subjected to loads in other directions. In addition, it is also established in the literature that 3D-printed parts are generally weaker between layers. Interlayer properties are often determined with the use of single-layer, vertically built specimens, as shown in Figure 12A. 129 We analyzed the in-plane and interlayer tensile strength of short fiber-reinforced composites using 57 data points (Figure 12). The highest tensile strength found in the literature was achieved by Allum et al., 130 who state that poor interlayer properties are not due to insufficient polymer bonding but due to geometric features. However, their claim contradicts other sources and may require further verification. König et al. 104 investigated the effects of process parameters on the interlayer bonding of carbon fiber-reinforced PA composites. The authors found that the carbon fibers decrease interlayer bonding strength, probably due to weak fiber-matrix adhesion. Bhandari et al. 131 found that carbon fibers reduce interlayer tensile strength by 66% and 50% for an amorphous and a semi-crystalline polymer, respectively. Post-processing increases strength but also increases production time and can deform 3D-printed products. The authors reported that

FIGURE 12 In-plane and interlayer tensile properties (A) interpretation of the directions, (B) in-plane and interlayer tensile strength as a function of their density, (C) Comparison of the tensile strength difference  $(\Delta\sigma_m = \sigma_{m,in\text{-plane}} - \sigma_{m,interlayer})$  of neat and composite structures. <sup>75,104,113,130,131,135–140</sup>

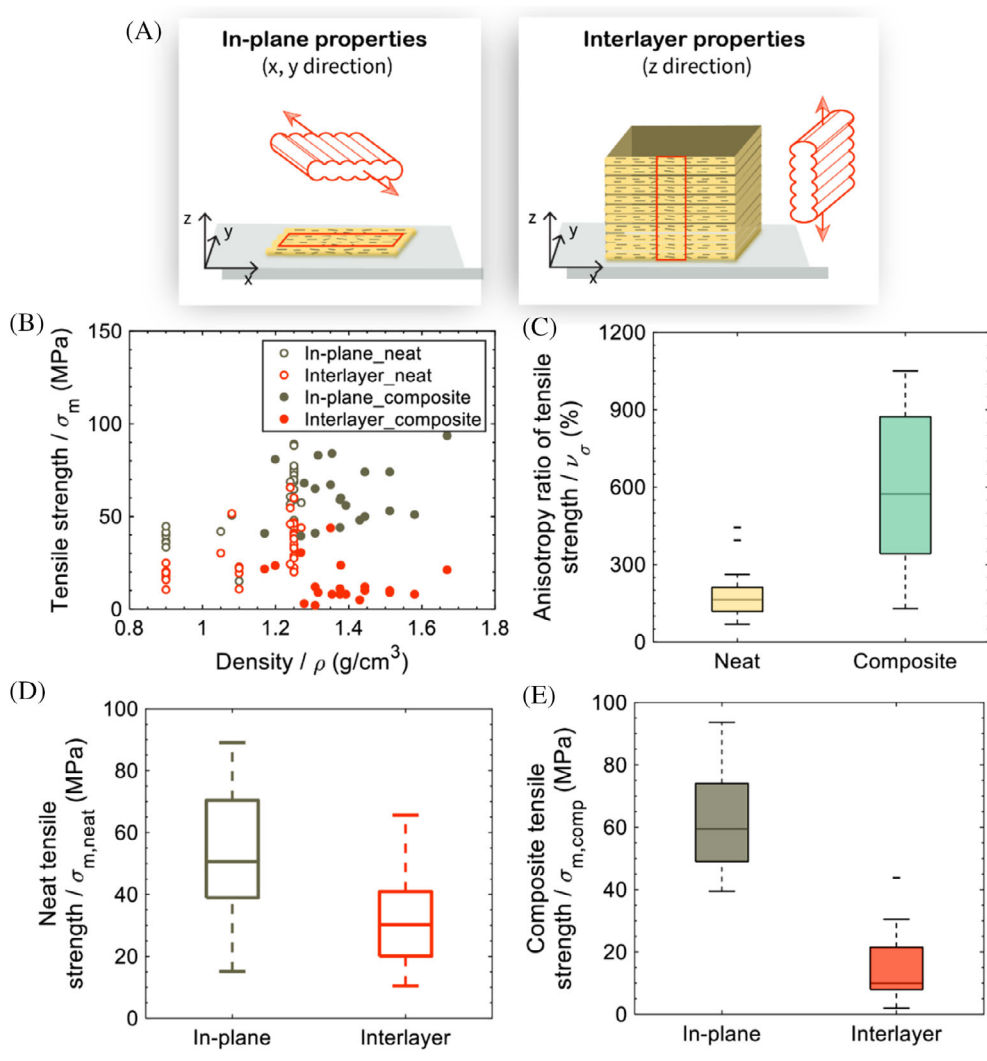


**TABLE 9** Median tensile strength and modulus values for the neat and composite 3D-printed materials.

	Neat		Composite	
Group	Number of data points	Median value of tensile strength (MPa)	Number of data points	Median value of tensile strength (MPa)
In-plane	37	53	20	62
Interlayer	37	31	20	14

increased melt viscosity and crystallization inhibit diffusion between layers and can therefore result in poor interlayer bond strength.

To compare the in-plane and interlayer tensile strength of the neat and fiber-reinforced materials (Figure 12B,D, E), we performed a Wilcoxon signed-rank test and a paired T-test, respectively. The median values of each group can be seen in Table 9. The statistical analysis showed that in-plane tensile strength was significantly higher than interlayer tensile strength for both the neat materials (p < 0.001) and the composites (p < 0.001). This confirms that the poor interlayer properties of 3D-printed structures

also occur in 3D-printed fiber-reinforced composites. To rate the difference between the in-plane and interlayer tensile strength of the 3D printed parts, we introduce the anisotropy ratio of tensile strength ( $\nu_{\sigma}$ ) which is the ratio of the in-plane and interlayer tensile strength ( $\nu_{\sigma} = \sigma_{\text{in-plane}}/\sigma_{\text{interlayer}}$ ) (Figure 12C). A Mann–Whitney test shows that  $\nu_{\sigma}$  for the composites is significantly higher than for the neat parts (p < 0.001). In terms of median values, the anisotropy ratio for composites and neat materials is 573% and 164%, respectively, that is, the addition of short fibers more than triples the anisotropy of the 3D printed parts. This type of anisotropy can be disadvantageous

because it limits the mechanical performance of the printed parts to one direction and makes the components vulnerable to stress in the out-of-plane direction. This can lead to reduced structural integrity, unpredictability in load-bearing applications, and potentially premature failure. To overcome anisotropy, advanced 3D-printing strategies are utilized, such as multi-axis printing  $^{132}$  or the "z-pinning" approach.  $^{133}$  These processes are based on the use of out-of-plane toolpaths, which allow for the continuous deposition of material in the building direction (z direction). Another solution to anisotropy could be to incorporate additional reinforcing materials between the layers.  $^{134}$ 

# 6 | MECHANICAL MODELS AND APPLICATIONS

Analytical models are widely used to predict the mechanical properties of 3D-printed short fiber-reinforced thermoplastic composites. The fibers are mostly applied to enhance the tensile, flexural, and other mechanical properties. The development of functional materials with conductive properties, shape memory capabilities, or biocompatibility is also gaining ground.

Fiber properties such as fiber length, fiber orientation, and fiber–matrix adhesion determine the mechanical properties and, therefore, need to be incorporated into predictive calculations. In analytical modeling, homogenization methods are usually used to treat composite materials as a single medium rather than analyzing the interaction of individual fibers and the matrix separately. These methods average the properties of the composite constituents (fiber and matrix) to give an overall estimate of mechanical behavior. By simplifying the complex microstructure of the composite, homogenization methods facilitate the prediction of overall material behavior, although they may not fully capture local variations in properties. However, microstructural properties have little predictability. <sup>105</sup>

Accurate modeling requires sufficient quantitative data on fiber properties, which can be time-consuming and prone to error. Analytical models are particularly useful when computational resources are limited or when fast, approximate predictions are needed at an early stage of design. Therefore, predicting the evolution of microstructural features as a function of manufacturing parameters and material properties could be an important future research direction.

# **6.1** | Microstructure and correction factors

There are many ways to quantify microstructural features, and the method chosen can greatly affect the

accuracy of the predictions. Table 10 summarizes the main microstructural features of short fiber-reinforced composites, and the quantitative measures of the features and their common calculation methods. Figure 13 shows schematics of the features. Average fiber length can be expressed as a numerical (Equation 10) or a lengthweighted average (Equation 11) of the length of the individual fibers. Fiber length can also be characterized by a distribution function, for which a Weibull distribution is most often used (Equation 12). Similarly, the orientation of each fiber can be averaged and is given by the principal diagonal values of the second-order orientation tensor in the 3 main directions (Equation 13). A more precise way of specifying this can be the fiber orientation distribution function (FOD). Many specific probability density functions are used in the literature to describe orientation.<sup>141</sup> Equation 14 shows a single-parameter exponential function presented by Chin et al<sup>142</sup> regarding orientation.

Fiber length distribution (FLD) can be determined as follows. After burning off the matrix or chemically dissolving it, the remaining fibers are dispersed and placed under an optical microscope. Images of the fibers are captured, and image analysis software is used to measure the length of individual fibers. The method is direct but can be timeconsuming. In some cases, researchers have found that the use of length averages in mechanical modeling procedures can provide a sufficiently accurate estimate, which can reduce the computational capacity required. 142,143 To measure the FOD, often a polished surface is prepared, and the orientation is determined based on the geometry of the fiber cross-sections (Figure 14C). The directional arrangement of the fibers might also be detected indirectly, based on their functional properties.<sup>124</sup> If the electrical conductivity<sup>144</sup> or the thermal conductivity<sup>145</sup> of the composite is higher in one direction, this indicates a higher degree of fiber orientation in that direction.

Regarding porosity, the simplest way to approximate void content is via density measurement (Equation 16). Scanning electron microscopic or optical microscopic images are also often used. The state-of-the-art technique to characterize the microstructure of composites is microtomography, which can provide the length, the 3D orientation of the fiber, and the distribution of voids in a non-destructive way. Data is obtained by collecting 2D projection images, from which the 3D structure can be reconstructed. The main components of the structure (matrix, fibers and voids) can be identified by image segmentation (Figure 14A). Tikhani et al. 106 determined fiber orientation using tomography data by applying a plane and calculating the orientation of the fibers intersecting it (Figure 14D). Nikolaou et al. 146 applied a segmentation process based on neural network algorithms (Figure 14B), which supported the accuracy of further mechanical modeling.

TABLE 10 Main microstructural features, their quantitative measures, and common calculation methods. 147-152

Feature	Quantification/ca	alculation method	Parameters
Fiber length	Equation 10 Equation 11 Equation 12	$\begin{split} L_n &= \frac{\sum_{n_i} n_i l_i}{n_i} \\ L_w &= \frac{\sum_{n_i} n_i l_i^2}{n_i} \\ f(l \mid a, b) &= \frac{b}{a} \left( \frac{x}{a} \right)^{b-1} e^{-\left( \frac{x}{a} \right)^b} \end{split}$	Number average fiber length (Ln) Length-weighted fiber length (Lw) Number of fibers (ni) Individual fiber lengths (li) Fiber length distribution function (f(l)) Weibull parameters (a, b)
Fiber orientation	Equation 13 Equation 14	$A_{ij} = egin{bmatrix} a_{xx} & a_{xy} & a_{xz} \ a_{yx} & a_{yy} & a_{yz} \ a_{zx} & a_{zy} & a_{zz} \end{bmatrix} \ g( heta;\lambda) = rac{\lambda \exp(-\lambda  heta)}{1-\exp(-rac{\lambda  au}{2})}  onumber $	Orientation tensor $(A_{ij})$ Fiber orientation distribution function $(g(\theta; \lambda))$
Fiber content	Equation 15	$v_f = rac{V_f}{V_c} = rac{rac{m_f}{ ho_f}}{rac{m_f}{ ho_f} + rac{m_m}{ ho_m}}$	Mass of fiber and matrix $(m_f, m_m)$ Density of fiber and matrix $(\rho_f, \rho_m)$ Fiber volume fraction $(v_f)$
Void content	Equation 16	$v_{v}=100- ho_{c}^{m}\Big(rac{W_{m}}{ ho_{m}}-rac{W_{f}}{ ho_{f}}\Big)$	Void volume fraction $(v_v)$ Measured composite density $(\rho_c^m)$ Weight percentage of matrix and fiber $(W_m, W_f)$ Density of matrix and fiber $(\rho_m, \rho_f)$
Fiber-matrix interfacial adhesion	Equation 17	$ au = rac{\sigma_f d_f}{2L_c}$	Interfacial shear strength $(\tau)$ Tensile strength of a single fiber $(\sigma_f)$ Fiber diameter $(d_f)$ Critical fiber length $(L_c)$

In micromechanical modeling of short fiber-reinforced composites, correction factors are applied to account for the microstructural effects that influence the overall behavior of the composite. Commonly used correction factors are shown in Table 11. These factors help bridge the gap between idealized models and real-world materials. Fiber length correction factors account for the reduced load transfer efficiency in short fibers compared to continuous fibers, as short fibers do not fully develop their potential tensile strength due to insufficient bonding length with the matrix. They are used for strength and stiffness predictions. Since fibers in short fiberreinforced composites are often randomly oriented or aligned in specific patterns, orientation factors can adjust models to account for the actual fiber orientation distribution. The composite's properties will vary depending on the alignment of the fibers relative to the load direction, and this factor modifies the model to reflect that anisotropy (Equation 18, 19).

The fiber geometry factor (Equation 20) is a parameter that takes into account the shape and distribution of fibers in the composite and is intended to describe how stress is transferred from the matrix to the fibers. The fiber packing parameter (Equation 21) describes how fibers are distributed or packed within the matrix. The parameter accounts for how closely or loosely the fibers are arranged and how this arrangement affects the load distribution and the effectiveness of stress transfer

through the matrix. The geometry factor and fiber packing parameters are usually used in shear lag models. The fiber clustering parameter (Equation 22) accounts for the presence of fiber agglomerations. In short fiber-reinforced composites, fibers are often not perfectly dispersed; instead, they may form clusters due to processing conditions, fiber-fiber interactions, or inadequate mixing. The clusters reduce the stress transfer efficiency and can act as localized failure points.

Voids reduce the effective load-bearing area of the composite and can act as stress concentrators, lowering both stiffness and strength, therefore void factors compensate for the presence of voids or pores within the composite. At the lamina level, new variables are introduced that are bead orientation, intralayer bonding strength, and inter-bead void content. The degree of neck formation between the adjacent beads determines the horizontal bond width and thus controls the inter-bead void content. For mechanical modeling, the lamina is usually considered an orthotropic bead-void compound and the interbead void content can be calculated with knowledge of the geometry of the beads and diffusion length.<sup>153</sup> According to the Rodriquez formula, void content is given with Equation 23, where the voids are calculated with the geometry of the beads (m and n are thickness and height, respectively) and the diffusion length between the beads ( $\delta$ and  $\Delta$  are the vertical and horizontal lengths of the neck, respectively). 153,154

, Wiley Online Library on [21/08/2025]. See the Terms

FIGURE 13 Main microstructural features of short fiber-reinforced 3D-printed composites: Material properties, fiber length, fiber orientation, and void content.

# 6.2 | Mechanical models used for the prediction of tensile strength and Young's modulus

Micromechanical models are used to predict the tensile properties of short fiber-reinforced composites by considering the contributions of the individual components (fibers and matrix) as well as the effects of fiber length, orientation, distribution, fiber-matrix interface, and other microstructural factors. Commonly used models for short fiber-reinforced 3D-printed composites are shown in Table 12. The models typically rely on a few key assumptions, for example, some models assume perfect bonding between the fibers and matrix, while others introduce correction factors to account for imperfections or weak bonding. Many models assume that both the fibers and matrix behave elastically up to failure. Generally, the first step is determining the volume fractions of the fibers and matrix (Equation 15). Then, the five elastic constants can be calculated (Equations 24-28), which describe the directional behavior of the composite.

Zou et al.<sup>157</sup> developed constitutive models for isotropic and transversely isotropic elasticity to account for the anisotropy of neat 3D-printed polymers (Equation 29). The authors constructed a yield model to describe tensile strength in the case of different building orientations. If fibers are also present, one of the simplest models to predict mechanical properties is the Rule of Mixtures (RoM, Equation 30). The RoM assumes that properties of the composite are weighted averages of the properties of the fibers and the matrix. To improve accuracy, micromechanical models introduce various efficiency factors that account for the reduced load transfer efficiency due to fiber length, orientation, voids, and other imperfections. In the Halpin-Tsai model, fiber length and fiber orientation are considered correction factors (Equation 31). The Modified Kelly-Tyson model (Equation 32) is applied for tensile strength prediction, and it accounts for fiber orientation, length, and fiber-matrix adhesion. Yu et al.<sup>69</sup> applied the Kerner-Hashin model (Equation 33) to include the effects of voids in stiffness prediction. Cox's model, or the shear-lag model (Equation 34, 35) proposes that the effectiveness of load transfer in an aligned shortfiber composite is related to the modulus of both the fiber and the matrix. The contribution of the fiber is scaled by a fiber geometry factor ( $\lambda$ ), which represents the load

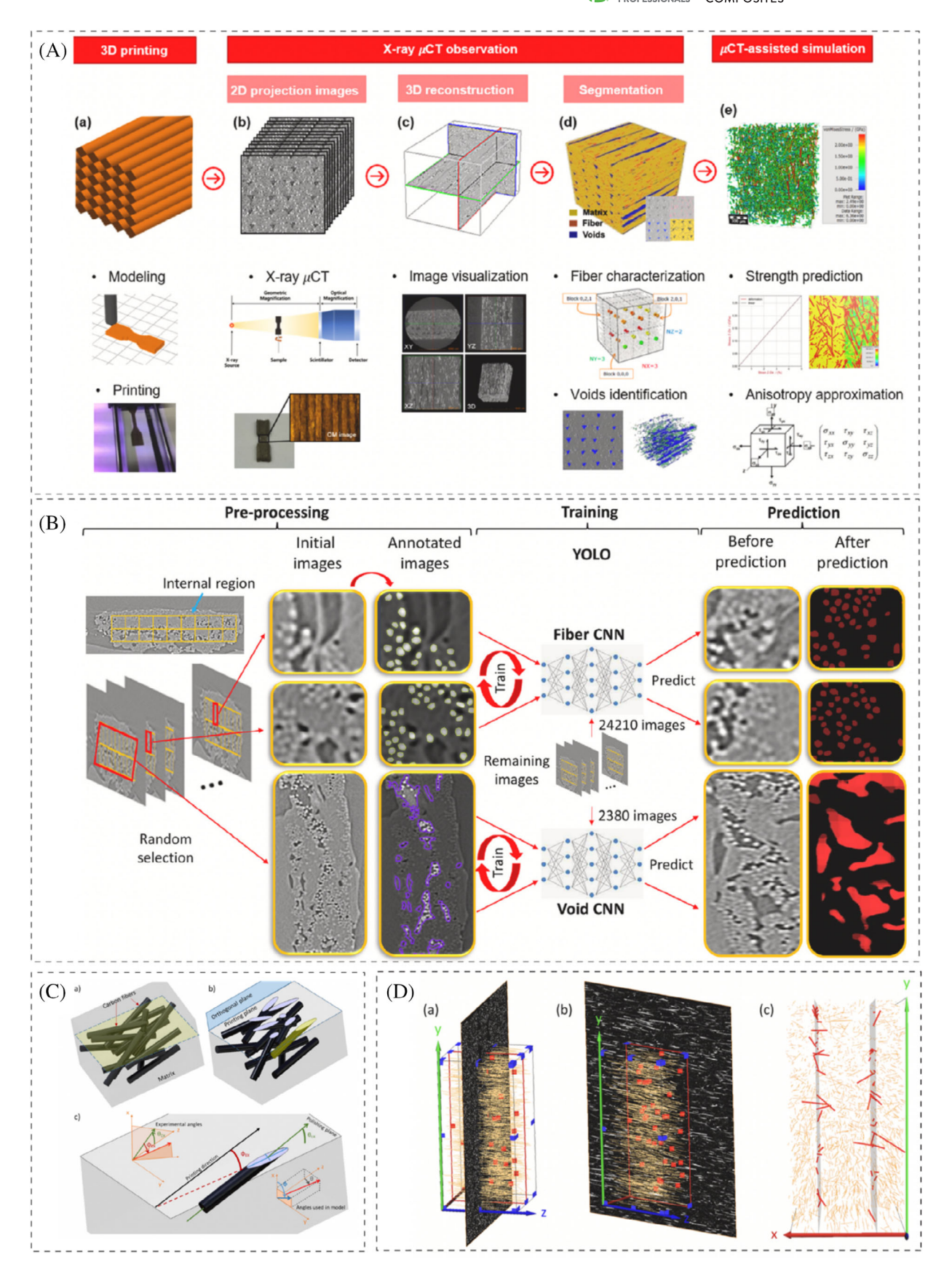


FIGURE 14 Measurement methods of microstructural properties (A) main components (matrix, fibers and voids) identified by image segmentation from tomography data<sup>98</sup> (B) segmentation process based on neural network algorithms<sup>146</sup> (C) measuring fiber orientation using cross-section geometry<sup>73</sup> (D) measuring fiber orientation using tomography data.<sup>106</sup>

onlinelibrary. wiley.com/doi/10.1002/pc.29850 by Budapest University of Technology and Economics, Wiley Online Library on [21/08/2025]. See the Terms and Conditions (https://onlinelibrary.wiley.com/doi/10.1002/pc.29850 by Budapest University of Technology and Economics, Wiley Online Library on [21/08/2025]. See the Terms and Conditions (https://onlinelibrary.wiley.com/doi/10.1002/pc.29850 by Budapest University of Technology and Economics, Wiley Online Library on [21/08/2025]. See the Terms and Conditions (https://onlinelibrary.wiley.com/doi/10.1002/pc.29850 by Budapest University of Technology and Economics, Wiley Online Library on [21/08/2025]. See the Terms and Conditions (https://onlinelibrary.wiley.com/doi/10.1002/pc.29850 by Budapest University of Technology and Economics, Wiley Online Library on [21/08/2025]. See the Terms and Conditions (https://onlinelibrary.wiley.com/doi/10.1002/pc.29850 by Budapest University of Technology and Economics, Wiley Online Library on [21/08/2025]. See the Terms and Conditions (https://onlinelibrary.wiley.com/doi/10.1002/pc.29850 by Budapest (https://onlinelibrary.wil

iditions) on Wiley Online Library for rules of use; OA articles are governed by the applicable Creative Commons

 TABLE 11
 Correction factors derived from microstructural features.

Microstructural feature	Correction fa	ctor	Components
Fiber length, Fiber orientation	Equation 18	$\begin{split} \chi_1 \chi_2 &= \int_{\theta_{min}}^{\theta_{max}} \int\limits_{l_{min}}^{l_c} f(l) g(\theta) (l/L_n) (l/2l_c) e^{(\mu \theta)} dl d\theta \\ &+ \int_{\theta_{min}}^{\theta_{max}} \int\limits_{l_c}^{l_{max}} \frac{f(l) g(\theta) (l/L_n) (1-A_f tan(\theta)) \times}{\left(1-l_c (1-A_f tan(\theta))/\left(2l e^{(\mu \theta)}\right)\right)} dl d\theta \end{split}$	$\begin{aligned} & \text{FLD } (f(l)) \\ & \text{FOD } (g(\theta)) \\ & \text{Critical fiber length } (l_c) \\ & \text{Average fiber length } (L_n) \\ & \text{Snubbing friction} \\ & \text{coefficient } (\mu) \\ & \text{Aonstant } (A_f) \end{aligned}$
Fiber orientation	Equation 19	$\chi_2 = \int_0^{\pi/2} h(\theta) \cos\theta d\theta \times \int_0^{\pi/2} h(\theta) (\cos^3\theta - \nu \sin^2\theta \cos\theta) d\theta$	FOD $(g(\theta))$ Poisson's ratio $(\nu)$
Fiber geometry	Equation 20	$\lambda = 1 - rac{ anh \left(rac{\eta_c l}{2} ight)}{rac{\eta_c l}{2}}$	Shear lag parameter $(\eta_c)$ Fiber length $(l)$
Fiber volume fraction (square packing)	Equation 21	$v = \frac{\pi r_f^2}{R^2}$	Fiber radius $(r_f)$ Side length of the enclosing square $(R)$
Fiber clustering	Equation 22	$lpha = 1 - rac{V_f}{V_{flbermax}}$	Fiber volume fraction $(V_f)$ Maximum fiber Volumetric fraction $(V_{fibermax})$
Void content	Equation 23	$V_{ u}=1-rac{\pi mn}{(2n-\delta)(2m-\Delta)}$	Bead geometry (m, n)

transfer efficiency with the ratio of the shear lag parameter ( $\eta_c$ ) and the fiber length (l). The shear lag parameter depends on the ratio of the Young's modulus of the fiber ( $E_f$ ) to the shear modulus ( $G_m$ ) of the matrix, as well as the fiber aspect ratio. The fiber volume fraction for square packing takes into account the mean center-to-center separation of the fibers ( $R_f$ ). The Eshelby-Mori-Tanaka model (Equation 36) combines Eshelby's inclusion problem with the Mori-Tanaka average stress approach to define the effective elastic properties of a heterogeneous two-phase material. As a general 3D-printed structure can be found analogous to composite laminates, the Classical Laminate Theory (CLT) can also be used at the laminate level (Equation 37).

Multiscale finite element models (FEM) are also gaining ground for short fiber-reinforced 3D-printed composites. Estefani and Távara<sup>162</sup> built a FEM model in which the integration points correspond to the centers of Representative Volume Elements (RVEs), and equivalent homogeneous properties are assigned based on these RVEs at the macro level. At the meso scale, RVEs represent the arrangement of beads, accounting for their orientation, layer order, and potential porosity, and using probability functions and boundary conditions to derive macro-level constitutive laws (Figure 15D). Gonabadi et al. 161 presented a multi-scale FE analysis in which, at the micro-scale, RVEs were modeled, taking into account volume fractions and fiber geometry. At the mezo-scale, voids between the beads were also considered. The FEA revealed local stresses at the fiber-matrix interface and at the bead-bead connections (Figure 15A). Bandinelli et al. 163 presented a FE model that accounts for

raster angle and building orientation. The authors showed that the elastoplastic behavior and the failure modes are influenced by the anisotropic nature of the 3D-printed parts. Cai et al. 164 reconstructed a simplified microscopic model using 3D parametric finite-volume direct averaging micromechanical theory based on statistical results from micro-CT data (Figure 15B). Lei et al. 165 applied a void array mapping method using scanning electron microscopy images to construct RVEs (Figure 15E). In this way, different void geometries specific for 3D-printed structures were taken into account in estimating stiffness. Yan et al. 166 presented a Modified Random Sequential Adsorption algorithm for the generation of RVEs. Besides the fiber properties (volume, length, orientation), the model also considers voids and foreign matter particles, which are of great importance for composites made with recycled fibers (Figure 15C). The model was verified on recycled glass fiber-reinforced PLA composites.

Table 13 shows the micromechanical models applied for 3D-printed short fiber-reinforced composites to predict tensile strength and Young's modulus in the literature. Yan et al. 156 evaluated the applicability of numerous classic micromechanical models for short fiber-reinforced 3D-printed composites. The RoM, modified rule of mixtures (MRoM), Kelly model, Cox shear lag model, and modified Cox models were used to predict the longitudinal strength and modulus. The RoM transverse model and bridging model were applied for transverse strength, and the RoM transverse model, Halpin-Tsai, and modified Halpin-Tsai models were used to predict the transverse modulus. The authors revealed that fiber orientation, fiber

Name	Model	ing tensile properties. <sup>69,147,151,158–161</sup>	Components
			Volume fraction of the fiber and
Material properties	Equation 24 Equation 25	$egin{align} E_1 = E_f  u_f + E_m ig( 1 -  u_f ig) \ E_2 = igg[ rac{ u_f}{E_f} + rac{(1 -  u_f)}{E_m} igg]^{-1} \ \end{split}$	the matrix $(v_f, v_m)$ Elastic modulus of the fiber and the matrix $(E_f, E_m)$
	Equation 26	$G_{12} = \left[rac{ u_f}{G_f} + rac{\left(1 -  u_f ight)}{G_m} ight]^{-1}$	Longitudinal elastic modulus (E <sub>1</sub> ) Transverse elastic modulus (E <sub>2</sub> )
	Equation 27	$\nu_{12} = v_f \nu_f + v_m \left( 1 - \nu_f \right)$	Shear modulus ( $G_{12}$ ) Poisson's ratio ( $\nu_{12}$ , $\nu_{21}$ )
	Equation 28	$ u_{21} = \frac{E_2}{E_1}  u_{12}$	1 01550113 14110 (112, 1121)
Transversely isotropic yielding model	Equation 29	$\sigma(\theta) = \sigma(0) + \left(\frac{\sigma(90) - \sigma(0)}{90}\right) \times \theta$	Building orientation angle ( $\theta$ ) Strength in the respective directions ( $\sigma(0), \sigma(90)$ )
Rule of Mixtures (RoM)	Equation 30	$\sigma_c = \sigma_f  u_{\!f} + \sigma_m ig(1 -  u_{\!f}ig)$	Strength of the composite $(\sigma_c)$ Fiber strength $(\sigma_f)$ Matrix strength $(\sigma_m)$
Halpin-Tsai	Equation 31	$\sigma_{ m c} = \chi_1 \chi_2 \sigma_f v_f + \sigma_m ig(1 - v_fig)$	Tensile strength of the composite $(\sigma_c)$ Tensile strength of fiber and matrix $(\sigma_f, \sigma_m)$ Length correction factor $(\chi_1)$ Orientation correction factor $(\chi_2)$
Kelly-Tyson	Equation 32	$\sigma_c = \eta_0 rac{ au L_f  u_f}{d_f} + E_m arepsilon_c \left(1 -  u_f ight)$	Tensile strength of the composite ( $\sigma_{tce}$ ) Fiber orientation factor ( $\eta_0$ ) Fiber length ( $L_f$ ) Fiber volume fraction ( $v_f$ ) Strain of the composite ( $\varepsilon_c$ )
Kerner-Hashin	Equation 33	$E_{me}=rac{9K_{me}G_{me}}{3K_{me}+G_{me}}$	Effective matrix modulus ( $E_{me}$ ) Effective shear modulus ( $G_{me}$ ) Effective bulk modulus ( $K_{me}$ )
Cox (shear lag)	Equation 34	$E_c = \lambda E_f \nu_f + E_m \left( 1 - \nu_f \right)$	Young's modulus of the composite $(E_c)$ Geometry factor $(\lambda)$
Cox (shear lag)	Equation 35	$\sigma_c = \lambda \sigma_f  u_f + \sigma_m ig(1 -  u_fig)$	Tensile strength of the composite $(\sigma_c)$ Geometry factor $(\lambda)$ Fiber volume fraction $(v_f)$ Tensile strength of fiber and matrix $(\sigma_f, \sigma_m)$
Eshelby-Mori- Tanaka	Equation 36	$D_{UDV} = \mathbf{D}_{UD} \{ (1 - V_V) (\mathbf{D}_V - \mathbf{D}_{UD}) \mathbf{S}_V + \mathbf{D}_{UD} \}^{-1} $ $\times [(1 - V_V) \{ (\mathbf{D}_V - \mathbf{D}_{UD}) \mathbf{S}_V + \mathbf{D}_{UD} \} + V_V \mathbf{D}_V ]$	Elastic constant of voids $(D_V)$ Void volume fraction $(V_V)$ Eshelby tensor $(S_V)$
Classical Laminate Theory (CLT)	Equation 37	$egin{aligned} \left[Q_{ij} ight] = egin{bmatrix} Q_{11} & Q_{12} & 0 \ Q_{12} & Q_{22} & 0 \ 0 & 0 & Q_{66} \end{bmatrix} \end{aligned}$	Tensor components $(Q_{xy})$

length, porosity, fiber clustering and weak fiber-matrix interface bonding are the main sources of inaccuracy. Yu et al.<sup>69</sup> applied the Kerner-Hashin method for the prediction of tensile strength and stiffness of basalt fiberreinforced PLA, and reported good agreement. Using the

Halpin-Tsai model, van de Werken et al.<sup>3</sup> found good agreement with experimental results measured on short carbon fiber-reinforced ABS composites. Pei et al. 105 applied the Halpin-Tsai model with data-driven parameter calibration, where fiber and void volume fractions were

onlinelibrary.wiley.com/doi/10.1002/pc.29850 by Budapest University of Technology and Economics, Wiley Online Library on [21/08/2025]. See the Terms

FIGURE 15 Representative Volume Elements (RVEs) modeled for 3D-printed short fiber–reinforced composites (A) Micro-, meso-, and macroscale model elements <sup>161</sup> (B) Microscopic model reconstructed from microtomography images <sup>164</sup> (C) RVE containing matrix, fibers, voids, and foreign particles from recycled fibers <sup>166</sup> (D) RVE considering fiber orientation and layer order <sup>162</sup> (E) Void array mapping method to prepare RVEs using scanning electron microscopy images. <sup>165</sup>

TABLE 13 Methods to estimate the tensile strength and Young's modulus in the literature. Filled cells contain the measurement method used, 'o' indicates that the property was approximated and ' $\times$ ' means that the property was not considered.

Modeled	Model amilied	Fihor lonath	Fiber	Fiber-matrix	Void content	Other	Cource
property	Model applied	riber iengui	orientation	aunesion	void content	Office	aonice
Tensile	Halpin-Tsai	microscopy	from surface	Ō	×	×	Werken et al. $2020^3$
strength	Halpin-Tsai	burnoff	0	0	×	×	<i>Tóth</i> et al. $2024^{75}$
	Halpin-Tsai	burnoff	x-ray microscopy	micro-droplet	×	×	<i>Tóth</i> et al. 2022 <sup>167</sup>
	MROM	burnoff	×	micro-droplet	×	×	<i>Tóth</i> et al. 2022 <sup>167</sup>
	Kelly-Tyson	x-ray microscopy	x-ray microscopy	0	x-ray microscopy	×	<i>Yu</i> et al. 2019 <sup>69</sup>
Young's	Eshelby-Mori-Tanaka	burnoff	×	×	×	×	<i>Shirasu</i> et al. 2024 <sup>168</sup>
modulus	Mori-Tanaka	burnoff	from surface	0	×		Abderrafai et al. $2022^{73}$
	Custom (Mori-Tanaka)	burnoff	from surface	0	×	bead shape	<i>Gupta</i> et al. 2022 <sup>169</sup>
	Modified shear lag	burnoff	×	×	×	×	Shirasu et al. $2024^{168}$
	Halpin-Tsai	burnoff	0	0	×	×	<i>Tóth</i> et al. $2024^{75}$
	Halpin-Tsai	microscopy	from surface	0	×	×	Werken et al. $2020^3$
	Halpin-Tsai, uncertainty analysis	microscopy	microscopy	×	microscopy	×	<i>Pei</i> et al. $202I^{105}$
	Stochastic modeling (MROM, CLT, PCE)	microscopy	0	×	microscopy	bead shape	<i>Papon</i> et al. 2019 <sup>154</sup>
	CLT	×	0	×	×	×	Somireddy et al. $2020^{170}$
	Custom micromechanical model	burnoff	from surface	×	x-ray microscopy	×	<i>Shirasu</i> et al. 2024 <sup>168</sup>

Note: A darker shade indicates that the property listed in the first row has been experimentally determined. A lighter shade indicates that the property has been approximated.

considered stochastic variables. They also analyzed the effects of process parameters on the structure. The authors revealed a structure-property relationship between void distribution and Young's modulus. Shirasu et al.<sup>51</sup> applied the Eshelby-Mori-Tanaka model to 3D-printed composites to account for void volume fraction and reported that it can approximate the stress-strain response well. Gupta et al.<sup>66</sup> applied the Mori-Tanaka approach with a two-step homogenization framework to predict Young's modulus and tensile strength as a function of fiber content. For homogenization, they considered and determined fiber length and bead size (the diameter of a single 3D-printed extrudate) experimentally. They found that the method reduces the error mostly for higher fiber contents, in the case of carbon fiber-reinforced polycarbonate composites. Abderrafai et al.73 also presented homogenization based on the Mori-Tanaka model to predict the Young's modulus of carbon fiber-reinforced polyamide composites. The authors showed that their method provides a lower bound for mechanical properties and that experimental values below this bound indicate imperfect fibermatrix adhesion. The CLT is applied mostly for continuous fiber-reinforced composites; for short fiber-reinforced composites, it is less used. Somireddy et al.<sup>58</sup> applied the CLT and the Tsai-Hill failure criteria and found that the voids degrade mechanical properties and reduce the accuracy of predictive methods. Papon et al.<sup>53</sup> identified three types of voids and considered their effects in a multi-level analytical modeling framework. They found that void distribution can be obtained from stochastic void models, and it can be used with the CLT to give accurate predictions for the overall laminate properties.

Overall, 5 cases of tensile strength modeling and 10 cases of micromechanical modeling for modulus estimation are presented, from a total of 10 literature sources. Fiber length is almost always incorporated as an empirical correction factor. Fiber orientation is also often measured, but in some cases, an approximate value is used based on the fact that fiber orientation corresponding to the printing direction is well established in the literature. Fiber-matrix adhesion is rarely incorporated, despite the fact that estimation inaccuracies are often attributed to inadequate adhesion. This may be because the interfacial shear strength that characterizes fibermatrix adhesion can only be given by time-consuming and error-prone measurement procedures empirically. Void content is only considered for modulus predictions. For strength, a lower accuracy of micromechanical methods is expected. Strength is a minimum value and a characteristic of the failure process, which is the result of several statistical processes and cannot be expected to be estimated by solely analytical approaches. The methods, however, provide order can magnitude

approximations, which can justify further calculations based on finite element methods coupled with failure criteria.

## 7 | NON-FIBROUS, WASTE-DERIVED REINFORCEMENTS

The conversion of waste into filler material for thermoplastic matrices in 3D extrusion is a novel approach that reduces the use of primary raw materials and thus contributes to sustainability. Various types of waste are used, including agricultural by-products (e.g., rice husk, wheat straw or biochar from biomass), industrial residues (e.g., fly ash, slag or recycled glass) and polymer or composite waste (e.g., electronic waste, ground tire rubber). The waste is usually processed into fine granules by grinding, pyrolysis, or chemical treatment (Figure 16). Surface treatments or coupling agents are also often used to improve the bonding with the thermoplastic matrix.

# 7.1 | Fillers derived from agricultural byproducts

Fillers derived from agricultural waste are renewable and biodegradable; therefore, they are attractive for sustainable composite development. Various types have been used as fillers for 3D-printed composites, such as tomato stem, <sup>171</sup> coffee grounds, <sup>172–174</sup> rice husk <sup>175</sup> or chicken feather. <sup>176</sup> Agricultural byproducts are organic materials that exhibit inconsistent mechanical properties. Due to their irregular shape, particle size distribution, and surface characteristics, these fillers often cause random changes and can even reduce the overall mechanical properties. Pemas et al. 171 created 3D-printed filament from PLA pellet and added 0, 5, and 10 wt% of tomato stem powder (TSP) with particles smaller than 150 µm. Their results show that increasing the TSP ratio decreases the tensile and flexural strength, as well as the elongation at break. The tensile and flexural modulus did not increase with TSP addition. Morales et al. 175 prepared filaments with recycled polypropylene (rPP) and rice husk (RH) powder with a particle size between 250 and 425 µm. They found that the tensile strength, elongation at break, and Young's modulus decreased with increasing RH content.

However, agricultural waste fillers have also been reported to increase the mechanical properties of thermoplastic matrices. Sotohou et al. 177 prepared 3D printed rPP specimens filled with 5 and 10 wt% bean pods powder (BPP). They found that the BPP increased the tensile strength and the compression strength by 10%, and it increased the flexural strength by 20%. Research shows



FIGURE 16 Agricultural and multicomponent waste as fillers: (A) tomato stem powder, (B) ground coffee, (C) grinded aluminum-plastic packaging, (D) grinded waste rubber. 171,173,188,194

that in most cases, biochar increases the mechanical properties. Biochar is a carbon-rich material derived from biomass through pyrolysis. Its particle size typically ranges from nano to micrometer scales. However, in most cases, the increase is not trend-like, so it is difficult to predict the property-modifying effect. Idrees et al. 178 prepared 3D printed composite samples from recycled poly(ethylene terephthalate) (rPET) bottles and 0, 1, 3, and 5 wt% biochar. The latter was derived from the pyrolysis of packaging waste. Adding biochar significantly increased (around 30%) both tensile strength and Young's modulus in all cases, but no trend-like changes were observed as a function of filler content. Zaheeruddin et al. 179 created 3D printed composites

from PP and biochar derived from the pyrolysis of packaging waste. The biochar addition significantly increased both tensile strength and Young's modulus in all cases, while no trend-like changes in strength as a function of filler content were observed. Vidakis et al. 180 prepared 3D printed composites from high-density polyethylene (HDPE) and biochar, which was produced by flame-curtain pyrolysis of olive tree prunings. Biochar doping significantly increased both tensile strength and Young's modulus in all cases, but no trend-like changes were observed as a function of filler content. Overall, the many benefits of biochar as a filler have been demonstrated, but further studies are needed to understand

1548/569, 0, Downloaded from https://4spepublications.onlinelibrary.wiley.com/doi/10.1002/pc.29850 by Buldpest University of Technology and Economics, Wiley Online Library on [21/08/2025]. See the Terms and Conditions (https://onlinelibrary.wiley.com/etons.onlinelibrary.wiley

its effects on 3D printed structures, such as interlayer bond strength and void formation. <sup>181</sup>

Agricultural waste fillers are typically hydrophilic due to the presence of polar functional groups (e.g., hydroxyl, carboxyl). Therefore, they are prone to moisture absorption, which can degrade the filler-polymer interface, reduce the mechanical properties of the composite, and affect dimensional stability. They can also aggregate easily, which causes stress accumulation sites in the composite. Without chemical modifications (e.g., coupling agents or surface treatments), these fillers have limited compatibility with non-polar polymer matrices, leading to weak interfacial adhesion. Carmona-Cabello et al.<sup>182</sup> prepared 3D printed ABS specimens filled with corn straw waste (CSW). To facilitate mixing between ABS and CSW, they used 1 wt% glycerol. The Young's modulus increased slightly (11% at best) and the flexural modulus increased significantly.

# 7.2 | Multi-component and industrial waste

Recycling of multi-component waste is challenging due to the diverse composition, which may contain incompatible polymers, additives, and contaminants. This heterogeneity makes separation, cleaning, and recycling difficult. Grinded multi-component waste often consists of irregularly shaped particles with a wide size distribution. In addition, there are several types of homogeneous industrial waste, the recycling of which is a complex task. Crosslinked polymers such as epoxy resins or vulcanized rubbers cannot be easily remelted or reprocessed due to their permanent chemical bonds. Therefore, they are often used as fillers in grinded or powdered form. Waste tire rubber particles were found to increase the mechanical performance of 3D-printed composites, especially the damping properties. 183-185 However, the property modification effects of crosslinked polymer fillers are not always positive due to their incompatibility with the thermoplastic matrix. Gama et al. 186 mixed polyurethane foam residues with TPU and found that with higher filler content, the mechanical performance decreased.

Electronic waste (e-waste) fillers are derived from diverse materials with mixed compositions (e.g., polymers, metals, ceramics). E-waste fillers may not disperse uniformly in the polymer matrix due to varying particle sizes, shapes, and densities. Gaikwad et al. <sup>187</sup> prepared polycarbonate (PC) specimens from electronic waste (specifically from end-of-life printers) and compared its mechanical properties to virgin ABS specimens. Regarding the tensile properties, e-waste PC specimens exhibited up to 76% and 83% of the breaking and tensile strength compared to the ABS ones. Spirio et al. <sup>188</sup> presented a strategy for the recovery of a typical e-waste plastic stream consisting of

polypropylene recovered from small appliances, mainly filled with talc particles. The recycled material was suitable for material extrusion 3D printing. Other multi-component wastes have also been found to be suitable as fillers, such as wind turbine blades<sup>189,190</sup> aluminum-plastic packaging waste<sup>191</sup> and textiles.<sup>192,193</sup>

# 7.3 | Microstructure of particle-filled composites

Chopped fibers consist of discrete, elongated fibers with an aspect ratio (length-to-diameter ratio) greater than 10. The fibers, especially if not recycled, generally maintain a relatively high degree of structural integrity. Compared to them, fillers derived from waste are composed of irregular, often fine particles with a much lower aspect ratio (typically closer to 1), usually without a main geometric dimension. 3D-printed composites containing particulate fillers generally do not have a primary orientation in the particles, unlike fiber-reinforced composites where the fibers are aligned along specific directions. Instead, the distribution of particles is rather random. Therefore, the composites show more isotropic behavior. Since waste-derived fillers are typically produced by grinding and/or milling, the particle size distribution depends on the material composition and the milling parameters. Thus, besides monomodal distribution, bimodal or wide size range can also be achieved (Figure 17).

Mechanical modeling of 3D-printed particle-reinforced thermoplastic composites is based on the knowledge of microstructural properties, similar to fiber-reinforced composites. Homogenization methods such as the Cox or Mori-Tanaka approach and finite element representative volume element (RVE) analysis can be used to predict the effective properties. For example, Joyee et al. 195 found that Young's modulus of 3D printed particle-filled polymer composites can be modeled with the Cox-Krenchel model using a Carman-Reifsnider correction. Their results showed that for printing directions of 0 and 45°, the modeling error was less than 5.5% in all cases. The Mori-Tanaka method is computationally efficient but assumes perfect interfacial bonding and uniform distribution, which may not be representative of multicomponent 3D-printed structures. RVE analysis using finite element models provides the highest fidelity by directly simulating the microstructure by considering the shape, size, and distribution of the particles. However, this is computationally expensive and requires detailed microstructural data. Microstructural features such as particle size distribution, shape, and spatial arrangement are critical for accurate modeling and are measured using

, Wiley Online Library on [21/08/2025]. See the Terms and Conditions (https://onli

on Wiley Online Library for rules of use; OA articles are governed by the applicable Creative Commons

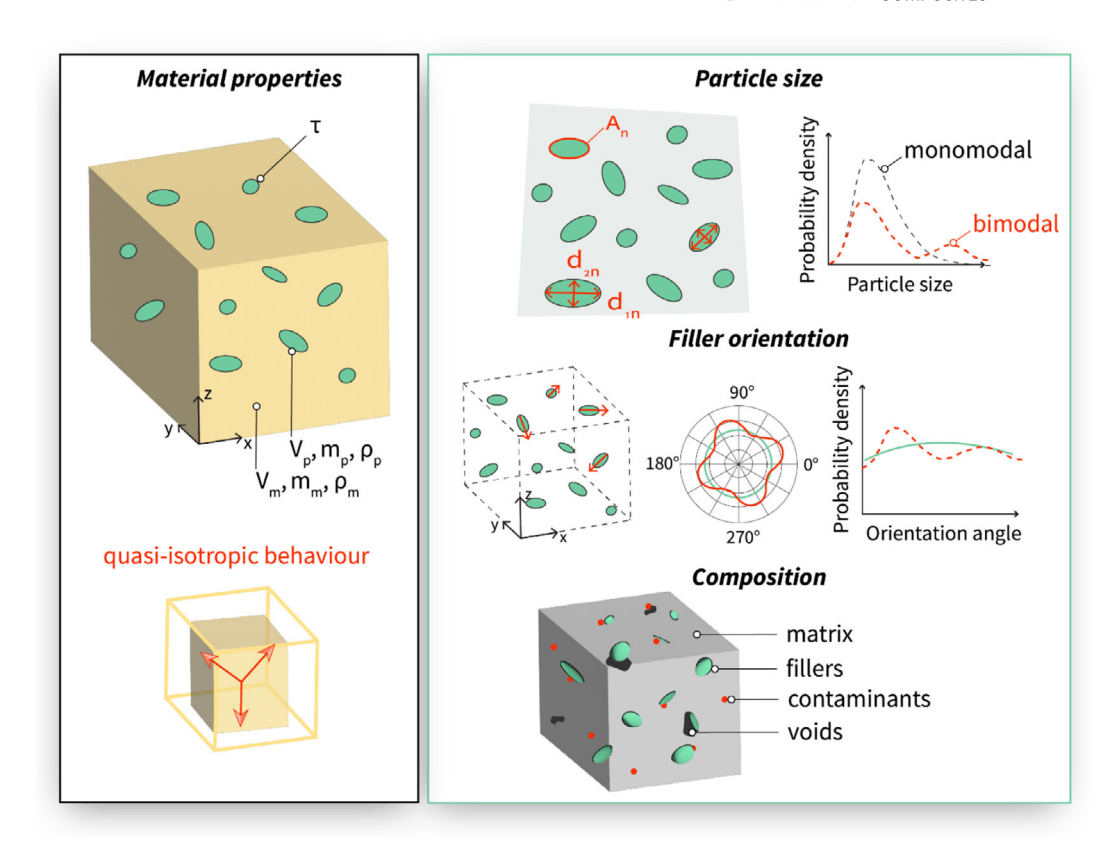


FIGURE 17 Main microstructural features of particle-filled 3D-printed composites: Material properties, particle size, orientation, and composition.

advanced imaging techniques. Although these techniques provide detailed input data for modeling, they can be labor intensive and sensitive to sample preparation, which emphasizes the importance of robust experimental protocols for reliable property prediction. <sup>196</sup>

# 8 | CONCLUSION AND FUTURE OUTLOOK

For short fiber-reinforced composites, based on the literature review, it can be concluded that the positive property-modifying effect of fibers is often not exploited. Moreover, in many cases, a deterioration of properties occurs. This is because the microstructural features that determine macroscale properties are not well designed, or not known at all. The main microstructural properties, fiber length, orientation, and void distribution are strongly influenced by the manufacturing conditions. Most fiber breakage occurs during the filament manufacturing process, and the rate of fragmentation is independent of both the fiber content and the initial fiber length. Therefore, in order to achieve longer fibers, the production method must be optimized by using fewer high-shear steps or by using gentler process parameters or screw configurations.

Analytical methods are emerging that incorporate these features to predict mechanical properties. For an accurate estimation, correction is performed using quantified microstructural features, but this requires a large number of time-consuming measurements. It would therefore be necessary to estimate the microstructure with the use of the manufacturing conditions and material properties. Furthermore, interlayer properties are surprisingly often neglected, even though the anisotropy of printed structures is a strong barrier to their application in engineering. Greater emphasis should also be placed on increasing fiber-matrix adhesion, for example, by using compatibilizers or by forming functional groups on the surface by beam or plasma treatment.

In the pursuit of sustainability, the use of waste materials (e.g., rice husk, biochar or electronic waste) as fillers is increasingly being used alongside traditional fiber reinforcements. The waste is usually processed into fine particles by grinding, which can result in a bimodal or wide size range in addition to a monomodal distribution. In terms of their microstructural characteristics, these waste particles are generally irregular in shape and have a low aspect ratio, with no major geometric dimension. Therefore, 3D printed composites filled with waste particles generally exhibit quasi-isotropic behavior.

The statistical analysis of the data collected from the literature revealed the following:

- · At the filament preparation stage, fiber content does not affect the remaining mean fiber length, and it is also independent of initial fiber length. This means that only the selection of manufacturing steps and parameters determines the remaining fiber length.
- It was shown that the fiber aspect ratio has no effect on tensile strength. However, based on general knowledge of composites (and the Kelly-Tyson formula), a close relationship between tensile strength and fiber length is expected. Therefore, the lack of dependence suggests that fiber-matrix adhesion was not sufficient in most of the studies. This finding is also supported by the fact that the increase in tensile strength due to the fibers is only  $1.25 \pm 0.5$  times on average.
- Despite the presumably weak fiber-matrix adhesion, the fibers increased the tensile modulus by a factor of 2.22  $\pm$  1.41 and the flexural modulus by a factor of 2.69  $\pm$  1.35 on average. This is because the quality of fiber-matrix adhesion is mostly deterministic in the failure process. However, the change in modulus as a function of fiber content has been statistically proven not to correlate.
- Based on the analysis of the in-plane and interlayer tensile strength data, it can be concluded that the addition of short fibers further increases the anisotropy of 3D-printed parts. In many applications, anisotropy is a drawback because it results in good mechanical performance only in the printing directions and makes the part weak in others.
- Microstructural properties are generally determined experimentally. The most often considered correction factor in micromechanical models is fiber length, followed by fiber orientation. In fewer models, the number of voids is also taken into account, usually with the FE method. Fiber-matrix adhesion is mostly neglected, leading to inaccuracies.

Advanced, multi-scale modeling techniques will be key to bridging the gap between microstructural features and macroscopic mechanical behavior, particularly those incorporating waste-derived fillers. However, the gap is quite wide. The final properties are the result of several processing parameters starting from filler preparation, so to estimate the properties of 3D printed products, several modeling steps are needed involving rheological and breakage models. The unique properties of waste-derived fillers, such as irregular shape, non-uniform distribution, and varying material composition, add complexity to the modeling process. With advances in computational capabilities, integrating microscopic and mesoscopic models with continuum-based methods provide can

comprehensive picture of filler-matrix interactions that affect mechanical performance. This also includes consideration of the effects of environmental factors, such as moisture uptake, degradation rate, and temperature changes, as thermoplastic matrices can be sensitive to environmental effects. Finally, machine learning and artificial intelligencebased approaches represent a transformative opportunity. Using large data sets from experimental and simulation results, artificial intelligence (AI) algorithms can improve the accuracy of predictive modeling, identify hidden patterns in microstructural behavior, and optimize printing parameters in real time. By combining artificial intelligence with traditional modeling, automated systems can adaptively control the manufacturing process, enabling more efficient use of waste fillers to create sustainable, highperformance composites.

### **ACKNOWLEDGMENTS**

Project no. TKP-6-6/PALY-2021 has been implemented with the support provided by the Ministry of Culture and Innovation of Hungary from the National Research, Development and Innovation Fund, financed under the TKP2021-NVA funding scheme. Csenge Tóth is thankful for the support of the EKÖP-24-4-I-BME-198 University Research Fellowship Programme and Ábris Dávid Virág is thankful for the support of the EKÖP-24-4-I-BME-201 University Research Fellowship Programme of the Ministry for Culture and Innovation from the source of the National Research, Development and Innovation Fund. Kolos Molnár was supported by the János Bolyai Scholarship of the Hungarian Academy of Sciences. The research reported in this paper was supported by the National Research, Development and Innovation Office (NRDI, Hungary) through grants K146236 and FK138501. Project no. 2022-2.1.1-NL-2022-00012 "National Laboratory for Cooperative Technologies" has been implemented with the support provided by the Ministry of Culture and Innovation of Hungary from the National Research, Development and Innovation Fund, financed under the National Laboratories funding scheme. The research reported in this paper was supported by the H2020-MSCA RISE No. 872152 - GREEN-MAP project of the European Union.

## DATA AVAILABILITY STATEMENT

The data that support the findings of this study are openly available in Mendeley Data, V1 at 10.17632/ dzc4n7xfdr.1, "MatEx\_shortfiber\_composites\_review".

## ORCID

*Csenge Tóth* https://orcid.org/0000-0002-8191-9056 Kolos Molnár https://orcid.org/0000-0002-9331-4652 Ábris Dávid Virág https://orcid.org/0000-0001-9308-1468

### REFERENCES

- Wang X, Jiang M, Zhou Z, Gou J, Hui D. 3D printing of polymer matrix composites: a review and prospective. *Compos B Eng.* 2017;110:442-458. doi:10.1016/j.compositesb. 2016.11.034
- Fallon JJ, McKnight SH, Bortner MJ. Highly loaded fiber filled polymers for material extrusion: a review of current understanding. Addit Manuf. 2019;30:100810. doi:10.1016/j. addma.2019.100810
- van de Werken N, Tekinalp H, Khanbolouki P, Ozcan S, Williams A, Tehrani M. Additively manufactured carbon fiberreinforced composites: state of the art and perspective. *Addit Manuf.* 2020;31:100962. doi:10.1016/j.addma.2019.100962
- Pazhamannil RV, Edacherian A. Property enhancement approaches of fused filament fabrication technology: a review. *Polym Eng Sci.* 2022;62:1356-1376. doi:10.1002/pen.25948
- Angelopoulos PM, Samouhos M, Taxiarchou M. Functional fillers in composite filaments for fused filament fabrication; a review. *Mater Today: Proc.* 2021;37:4031-4043. doi:10.1016/j. matpr.2020.07.069
- Fico D, Rizzo D, Casciaro R, Esposito Corcione C. A review of polymer-based materials for fused filament fabrication (FFF): focus on sustainability and recycled materials. *Polymers*. 2022; 14:1-33. doi:10.3390/polym14030465
- Adeniran O, Cong W, Aremu A. Material design factors in the additive manufacturing of carbon fiber reinforced plastic composites: a state-of-the-art review. *Adv Ind Manuf Eng.* 2022;5: 100100. doi:10.1016/j.aime.2022.100100
- Adil S, Lazoglu I. A review on additive manufacturing of carbon fiber-reinforced polymers: current methods, materials, mechanical properties, applications and challenges. *J Appl Polym Sci.* 2023;140:1-28. doi:10.1002/app.53476
- Xu X, Ren H, Chen S, Luo X, Zhao F, Xiong Y. Review on melt flow simulations for thermoplastics and their fiber reinforced composites in fused deposition modeling. *J Manuf Proc.* 2023;92:272-286. doi:10.1016/j.jmapro.2023.02.039
- Tao Y, Li P, Zhang J, Wang S, Shi SQ, Kong F. A review of fused filament fabrication of continuous natural fiber reinforced thermoplastic composites: techniques and materials. *Polym Compos.* 2023;44:8200-8222. doi:10.1002/pc.27477
- 11. Dey A, Roan Eagle IN, Yodo N. A review on filament materials for fused filament fabrication. *J Manuf Mater Proc.* 2021; 5:1-40. doi:10.3390/jmmp5030069
- 12. Singh S, Singh G, Prakash C, Ramakrishna S. Current status and future directions of fused filament fabrication. *J Manuf Proc.* 2020;55:288-306. doi:10.1016/j.jmapro.2020.04.049
- 13. Al Rashid A, Koç M. Fused filament fabrication process: a review of numerical simulation techniques. *Polymers*. 2021; 13(20):3534. doi:10.3390/polym13203534
- 14. Kumar S, Singh R, Singh TP, Batish A. Fused filament fabrication: a comprehensive review. *J Thermoplast Compos Mater*. 2020;36(2):794-814. doi:10.1177/0892705720970629
- 15. Gao X, Qi S, Kuang X, Su Y, Li J, Wang D. Fused filament fabrication of polymer materials: a review of interlayer bond. *Addit Manuf.* 2021;37:101658. doi:10.1016/j.addma.2020.101658
- 16. Shaqour B, Abuabiah M, Abdel-Fattah S, et al. Gaining a better understanding of the extrusion process in fused filament fabrication 3D printing: a review. *Int J Adv Manuf Technol*. 2021;114:1279-1291. doi:10.1007/s00170-021-06918-6

- 17. Yadav A, Rohru P, Babbar A, et al. Fused filament fabrication: a state-of-the-art review of the technology, materials, properties and defects. *Int J Interactive Des Manuf.* 2023;17:2867-2889. doi:10.1007/s12008-022-01026-5
- Tran TQ, Ng FL, Kai JTY, Feih S, Nai MLS. Tensile strength enhancement of fused filament fabrication printed parts: a review of process improvement approaches and respective impact. Additive Manufacturing. 2022;54:102724. doi:10.1016/j.addma.2022.102724
- Tao Y, Kong F, Li Z, et al. A review on voids of 3D printed parts by fused filament fabrication. *J Mater Res Technol*. 2021; 15:4860-4879. doi:10.1016/j.jmrt.2021.10.108
- Zanjanijam AR, Major I, Lyons JG, Lafont U, Devine DM. Fused filament fabrication of peek: a review of processstructure-property relationships. *Polymers*. 2020;12:1-29. doi: 10.3390/POLYM12081665
- 21. Harris M, Potgieter J, Archer R, Arif KM. Effect of material and process specific factors on the strength of printed parts in fused filament fabrication: a review of recent developments. *Materials*. 2019;12:1-35. doi:10.3390/ma12101664
- Cojocaru V, Frunzaverde D, Miclosina CO, Marginean G.
   The influence of the process parameters on the mechanical properties of PLA specimens produced by fused filament fabrication—a review. *Polymers*. 2022;14:1-23. doi:10.3390/polym14050886
- Peterson AM. Review of acrylonitrile butadiene styrene in fused filament fabrication: a plastics engineering-focused perspective. Addit Manuf. 2019;27:363-371. doi:10.1016/j.addma. 2019.03.030
- Pratama J, Cahyono SI, Suyitno S, et al. A review on reinforcement methods for polymeric materials processed using fused filament fabrication (Fff). *Polymers*. 2021;13:1-23. doi: 10.3390/polym13224022
- Pejak Simunec D, Sola A. Emerging research in conductive materials for fused filament fabrication: a critical review. Adv Eng Mater. 2022;24:1-34. doi:10.1002/adem.202101476
- 26. Dua R, Rashad Z, Spears J, Dunn G, Maxwell M. Applications of 3d-printed peek via fused filament fabrication: a systematic review. *Polymers*. 2021;13:1-15. doi:10.3390/polym13224046
- Fu Y, Downey A, Yuan L, Pratt A, Balogun Y. In situ monitoring for fused filament fabrication process: a review. *Addit Manuf.* 2021;38:101749. doi:10.1016/j.addma.2020.101749
- Pérez-Castillo JL, Cuan-Urquizo E, Roman-Flores A, et al. Curved layered fused filament fabrication: an overview. Addit Manuf. 2021;47:102354. doi:10.1016/j.addma.2021.102354
- Dickson AN, Abourayana HM, Dowling DP. 3D printing of fibre-reinforced thermoplastic composites using fused filament fabrication-a review. *Polymers*. 2020;12:1-18. doi:10. 3390/POLYM12102188
- Ahmadifar M, Benfriha K, Shirinbayan M, Tcharkhtchi A. Additive manufacturing of polymer-based composites using fused filament fabrication (FFF): a review. *Appl Compos Mater*. 2021;28:1335-1380. doi:10.1007/s10443-021-09933-8
- Zhang Y, Moon SK. Data-driven design strategy in fused filament fabrication: status and opportunities. *J Comput Des Eng.* 2021;8:489-509. doi:10.1093/jcde/qwaa094
- 32. Valvez S, Reis PNB, Susmel L, Berto F. Fused filament fabrication-4d-printed shape memory polymers: a review. *Polymers*. 2021;13:1-25. doi:10.3390/polym13050701

15480569, 0, Downloaded from https://4spepublications.onlinelibrary.wiley.com/doi/10.1002/pc.29850 by Budapest University of Technology and Economics, Wiley Online Library on [21/08/2025]. See the Terms and Conditions (https://onlinelibrary.wiley

of use; OA articles are governed by the applicable Creative Commons

- 33. Kaur G, Singari RM, Kumar H. A review of fused filament fabrication (FFF): process parameters and their impact on the tribological behavior of polymers (ABS). *Mater Today: Proc.* 2022;51:854-860. doi:10.1016/j.matpr.2021.06.274
- 34. Bakhtiari H, Aamir M, Tolouei-Rad M. Effect of 3D printing parameters on the fatigue properties of parts manufactured by fused filament fabrication: a review. *Appl Sci.* 2023;13(2):904. doi:10.3390/app13020904
- 35. Papon EA, Haque A. Review on process model, structure-property relationship of composites and future needs in fused filament fabrication. *J Reinf Plastics Compos.* 2020;39:758-789. doi:10.1177/0731684420929757
- Mohd Pu'ad NAS, Abdul Haq RH, Mohd Noh H, Abdullah HZ, Idris MI, Lee TC. Review on the fabrication of fused deposition modelling (FDM) composite filament for biomedical applications. *Mater Today: Proc.* 2020;29:228-232. doi: 10.1016/j.matpr.2020.05.535
- Sola A. Materials requirements in fused filament fabrication: a framework for the Design of Next-Generation 3D printable thermoplastics and composites. *Macromol Mater Eng.* 2022; 307:1-40. doi:10.1002/mame.202200197
- 38. Patel A, Taufik M. Nanocomposite materials for fused filament fabrication. *Mater Today: Proc.* 2021;47:5142-5150. doi: 10.1016/j.matpr.2021.05.438
- Mashayekhi F, Bardon J, Berthé V, Perrin H, Westermann S, Addiego F. Fused filament fabrication of polymers and continuous fiber-reinforced polymer composites: advances in structure optimization and health monitoring. *Polymers*. 2021;13:1-28. doi:10.3390/polym13050789
- Cai Z, Thirunavukkarasu N, Diao X, et al. Progress of polymer-based thermally conductive materials by fused filament fabrication: a comprehensive review. *Polymers*. 2022;14: 1-27. doi:10.3390/polym14204297
- 41. Wu Y, Wang K, Neto V, Peng Y, Valente R, Ahzi S. Interfacial behaviors of continuous carbon fiber reinforced polymers manufactured by fused filament fabrication: a review and prospect. *Int J Mater Forming*. 2022;15:1-18. doi:10.1007/s12289-022-01667-7
- Patterson AE, Chadha C, Jasiuk IM, Allison JT. Fracture testing of polymer materials processed via fused filament fabrication: a survey of materials, methods, and design applications.
   Prog Addit Manuf. 2021;6:765-780. doi:10.1007/s40964-021-00196-0
- 43. Vanaei HR, Shirinbayan M, Deligant M, Khelladi S, Tcharkhtchi A. In-process monitoring of temperature evolution during fused filament fabrication: a journey from numerical to experimental approaches. *Thermo*. 2021;1:332-360. doi: 10.3390/thermo1030021
- 44. Kristiawan RB, Imaduddin F, Ariawan D, Arifin Z. A Review on the Fused Deposition Modeling (FDM) 3D Printing: Filament Processing, Materials, and Printing Parameters. *Open Eng.* 2021;11(1):639-649. doi:10.1515/eng-2021-0063
- Mikula K, Skrzypczak D, Izydorczyk G, et al. 3D printing filament as a second life of waste plastics—a review. *Environ Sci Pollut Res.* 2021;28:12321-12333. doi:10.1007/s11356-020-10657-8
- 46. Tadi SP, Maddula SS, Mamilla RS. Sustainability aspects of composite filament fabrication for 3D printing applications.

- Renew Sustain Energy Rev. 2024;189:113961. doi:10.1016/j. rser.2023.113961
- 47. Krajangsawasdi N, Blok LG, Hamerton I, et al. Fused deposition modelling of fibre reinforced polymer composites: a parametric review. *J Compos Sci.* 2021;5:1-38. doi:10.3390/jcs5010029
- 48. Smith JA, Petersmann S, Arbeiter F, Schäfer U. Optimization and manufacture of polyetheretherketone patient specific cranial implants by material extrusion a clinical perspective. *J Mech Behav Biomed Mater*. 2023;144:1-25. doi:10.1016/j.jmbbm.2023.105965
- 49. Rothlauf S, Pieralli S, Wesemann C, et al. Influence of planning software and template design on the accuracy of static computer assisted implant surgery performed using guides fabricated with material extrusion technology: an in vitro study. *J Dent.* 2023;132:1-8. doi:10.1016/j.jdent.2023.104482
- 50. Güney A, Kernebeck L, Grijpma DW. 3D printing of porous poly(ε-caprolactone)-poly(trimethylene carbonate)-poly (ε-caprolactone) triblock copolymers and nano-apatite composite structures. *Express Polym Lett.* 2024;18:349-358. doi:10.3144/expresspolymlett.2024.26
- 51. da Siqueira A, da Silva Siqueira A, Ferreira Braga N, et al. Biodegradable scaffold: integration of polylactic acid, hydroxyapatite, and graphene oxide via FDM 3D printing. *Express Polym Lett.* 2024;18(6):656-672. doi:10.3144/expresspolymlett.2024.48
- Fruleux T, Castro M, Correa D, Wang K, Matsuzaki R, Duigou AL. Geometric limitations of 3D printed continuous flax-fiber reinforced biocomposites cellular lattice structures. Compos Part C: Open Access. 2022;9:100313. doi:10.1016/j. jcomc.2022.100313
- Chen Y, Ye L, Kinloch AJ, Zhang YX. 3D printed carbon-fibre reinforced composite lattice structures with good thermaldimensional stability. *Compos Sci Technol*. 2022;227:109599. doi:10.1016/j.compscitech.2022.109599
- Kiss-Nagy K, Simongáti G, Ficzere P. Investigation of 3D printed underwater thruster propellers using CFD and structural simulations. *Periodica Polytech Mech Eng.* 2024;68:70-77. doi:10.3311/PPme.23795
- Wang S, Lasn K. Integration of optical fibre sensors by material extrusion 3-D printing the effect of bottom interlayer thickness. *Mater Des.* 2022;221:110914. doi:10.1016/j.matdes. 2022.110914
- Mashayekhi F, Bardon J, Koutsawa Y, Westermann S, Addiego F. Methods for embedding fiber Bragg grating sensors during material extrusion: relationship between the interfacial bonding and strain transfer. *Addit Manuf.* 2023;68: 103497. doi:10.1016/j.addma.2023.103497
- Leber A, Dong C, Laperrousaz S, et al. Highly integrated multi-material fibers for soft robotics. Adv Sci. 2023;10:1-10. doi:10.1002/advs.202204016
- Yap YL, Sing SL, Yeong WY. A review of 3D printing processes and materials for soft robotics. *Rapid Prototyping J*. 2020;26:1345-1361. doi:10.1108/RPJ-11-2019-0302
- Verma P, Bansala T, Chauhan SS, Kumar D, Deveci S, Kumar S. Electromagnetic interference shielding performance of carbon nanostructure reinforced, 3D printed polymer composites. *J Mater Sci.* 2021;56:11769-11788. doi:10.1007/s10853-021-05985-0

- 60. Abedi K, Miri S, Gregorash L, Fayazbakhsh K. Evaluation of electromagnetic shielding properties of high-performance continuous carbon fiber composites fabricated by robotic 3D printing. *Addit Manuf.* 2022;54:102733. doi:10.1016/j.addma.2022.102733
- 61. Huttunen E, Nykänen MT, Alexandersen J. Material extrusion additive manufacturing and experimental testing of topology-optimised passive heat sinks using a thermally-conductive plastic filament. *Addit Manuf.* 2022;59:103123. doi:10.1016/j. addma.2022.103123
- 62. Guo Y, Yang H, Lin G, et al. Thermal performance of a 3D printed lattice-structure heat sink packaging phase change material. *Chin J Aeronaut*. 2021;34:373-385. doi:10.1016/j.cja. 2020.07.033
- 63. Liedl B, Höftberger T, Burgstaller C. Properties of multiple-processed natural short fiber polypropylene and Polylactic acid composites: a comparison. *Macromol.* 2024;4:723-738. doi:10.3390/macromol4040043
- Franzén B, Klason C, Kubát J, Kitano T. Fibre degradation during processing of short fibre reinforced thermoplastics. Composites. 1989;20:65-76. doi:10.1016/0010-4361(89)90684-8
- Boldizar A, Möller K. Degradation of ABS during repeated processing and accelerated ageing. *Polym Degrad Stab.* 2003; 81:359-366. doi:10.1016/S0141-3910(03)00107-1
- Nasirov A, Gupta A, Hasanov S, Fidan I. Three-scale asymptotic homogenization of short fiber reinforced additively manufactured polymer composites. *Compos B Eng.* 2020;202: 108269. doi:10.1016/J.COMPOSITESB.2020.108269
- 67. Yu S, Hwang YH, Lee KT, Kim SO, Hwang JY, Hong SH. Outstanding strengthening and toughening behavior of 3D-printed fiber-reinforced composites designed by biomimetic interfacial heterogeneity. Adv Sci. 2022;9:1-13. doi:10.1002/advs.202103561
- 68. Lu S, Zhang B, Niu J, et al. Effect of fiber content on mechanical properties of carbon fiber-reinforced polyetherether-ketone composites prepared using screw extrusionbased online mixing 3D printing. *Addit Manuf.* 2024;80: 103976. doi:10.1016/j.addma.2024.103976
- Yu S, Hwang YH, Hwang JY, Hong SH. Analytical study on the 3D-printed structure and mechanical properties of basalt fiber-reinforced PLA composites using X-ray microscopy. *Compos Sci Technol*. 2019;175:18-27. doi:10.1016/j.compscitech. 2019.03.005
- Sang L, Han S, Li Z, Yang X, Hou W. Development of short basalt fiber reinforced polylactide composites and their feasible evaluation for 3D printing applications. *Compos B Eng.* 2019;164:629-639. doi:10.1016/j.compositesb.2019.01.085
- Tekinalp HL, Kunc V, Velez-Garcia GM, et al. Highly oriented carbon fiber–polymer composites via additive manufacturing. *Compos Sci Technol.* 2014;105:144-150. doi:10.1016/J.COMP SCITECH.2014.10.009
- Giani N, Mazzocchetti L, Benelli T, Picchioni F, Giorgini L. Towards sustainability in 3D printing of thermoplastic composites: evaluation of recycled carbon fibers as reinforcing agent for FDM filament production and 3D printing. *Compos Part A: Appl Sci Manuf.* 2022;159:107002. doi:10.1016/j.compositesa.2022.107002
- 73. Abderrafai Y, Hadi Mahdavi M, et al. Additive manufacturing of short carbon fiber-reinforced polyamide composites by fused filament fabrication: formulation, manufacturing and

- characterization. *Mater Des.* 2022;214:110358. doi:10.1016/J. MATDES.2021.110358
- 74. Wang P, Zou B, Ding S, et al. Preparation of short CF/GF reinforced PEEK composite filaments and their comprehensive properties evaluation for FDM-3D printing. *Compos B Eng.* 2020;198:108175. doi:10.1016/j.compositesb.2020.108175
- Tóth C, Lukács NL, Kovács NK. The role of the fiber-matrix interface in the tensile properties of short fiber-reinforced 3Dprinted polylactic acid composites. *Polym Compos.* 2024; 45(15):13589-13602. doi:10.1002/pc.28720
- Fu Y-T, Li J, Li YQ, Fu SY, Guo FL. Full-process multi-scale morphological and mechanical analyses of 3D printed short carbon fiber reinforced polyetheretherketone composites. *Compos Sci Technol.* 2023;236:109999. doi:10.1016/j.compscitech.2023.109999
- 77. Sang L, Han S, Peng X, Jian X, Wang J. Development of 3D-printed basalt fiber reinforced thermoplastic honeycombs with enhanced compressive mechanical properties. *Compos Part A: Appl Sci Manuf.* 2019;125:105518. doi:10.1016/J. COMPOSITESA.2019.105518
- Shulga E, Karamov R, S. Sergeichev I, et al. Fused filament fabricated polypropylene composite reinforced by aligned glass fibers. *Materials*. 2020;13:1-9. doi:10.3390/MA13163442
- Coughlin N, Drake B, Fjerstad M, et al. Development and mechanical properties of basalt fiber-reinforced acrylonitrile butadiene styrene for in-space manufacturing applications. *J Compos Sci.* 2019;3:1-17. doi:10.3390/jcs3030089
- 80. Hua L, Wang X, Ding L, Zeng S, Liu J, Wu Z. Effects of fabrication parameters on the mechanical properties of short basalt-fiber-reinforced thermoplastic composites for fused deposition modeling-based 3D printing. *Polym Compos.* 2023; 44(6):3341-3357. doi:10.1002/pc.27325
- Shon K, Liu D, White JL. Experimental Studies and Modeling of Development of Dispersion and Fiber Damage in Continuous Compounding. *Int Polym Proc.* 2005;20(3):322-331. doi:10. 3139/217.1894
- 82. Inceoglu F, Ville J, Ghamri N, et al. Correlation between processing conditions and fiber breakage during compounding of glass fiber-reinforced polyamide. *Polym Compos.* 2011;32: 1842-1850. doi:10.1002/pc.21217
- 83. Durin A, de Micheli P, Ville J, Inceoglu F, Valette R, Vergnes B. A matricial approach of fibre breakage in twin-screw extrusion of glass fibres reinforced thermoplastics. *Compos Part A: Appl Sci Manuf.* 2013;48:47-56. doi:10.1016/j.compositesa.2012.12.011
- 84. Malatyali H, Schöppner V, Rabeneck N, Hanselle F, Austermeier L, Karch D. A model for the carbon fiber breakage along the twin-screw extruder. *SPE Polym.* 2021;2:145-152. doi:10.1002/pls2.10040
- 85. Schelleis C, Scheuring BM, Liebig WV, Hrymak AN, Henning F. Approaching polycarbonate as an LFT-D material: processing and mechanical properties. *Polymers*. 2023;15:1-24. doi:10.3390/polym15092041
- Höftberger T, Dietrich F, Zitzenbacher G, Burgstaller C. Influence of fiber content and dosing position on the the mechanical properties of short-carbon-fiber polypropylene compounds. *Polymers*. 2022;14:1-10. doi:10.3390/polym14224877
- 87. Yang Z, Yang Z, Chen H, Yan W. 3D printing of short fiber reinforced composites via material extrusion: fiber breakage. *Addit Manuf.* 2022;58:103067. doi:10.1016/j.addma.2022.103067

- 88. Hu Y, Ladani RB, Brandt M, Li Y, Mouritz AP. Carbon fibre damage during 3D printing of polymer matrix laminates using the FDM process. *Mater Des.* 2021;205:109679. doi:10.1016/j.matdes.2021.109679
- 89. Lingua A, Sosa-Rey F, Pautard S, Therriault D, Lévesque M. Multiscale characterization of the fracture mechanics of additively manufactured short fiber-reinforced composites. *Eng Fract Mech.* 2023;289:109343. doi:10.1016/j.engfracmech.2023. 109343
- 90. Duty C, Ajinjeru C, Kishore V, et al. What makes a material printable? A viscoelastic model for extrusion-based 3D printing of polymers. *J Manuf Proc.* 2018;35:526-537. doi:10.1016/j.jmapro.2018.08.008
- 91. Das A. Importance of polymer rheology on material extrusion additive manufacturing: correlating process physics to print properties. *ACS Appl Polym Mater.* 2021;3:1218-1249. doi:10. 1021/acsapm.0c01228
- Mackay ME. The importance of rheological behavior in the additive manufacturing technique material extrusion. *J Rheol*. 2018;62:1549-1561. doi:10.1122/1.5037687
- 93. Rabinowitsch B. Über die Viskosität und Elastizität von Solen. *Z Phys Chem.* 1929;145A(1):1-26. doi:10.1515/zpch-1929-14502
- 94. Bagley EB. End corrections in the capillary flow of polyethylene. *J Appl Phys.* 1957;28:624-627. doi:10.1063/1.1722814
- Zhang H, Zhang L, Wu J, An X, Yang D. Fibre Bridging and Nozzle Clogging in 3D Printing of Discontinuous Carbon Fibre-Reinforced Polymer Composites: Coupled CFD-DEM Modelling. *Int J Adv Manuf Technol.* 2021;117(11-12):3549-3562. doi:10. 1007/s00170-021-07913-7
- Spoerk M, Gonzalez-Gutierrez J, Sapkota J, Schuschnigg S, Holzer C. Effect of the printing bed temperature on the adhesion of parts produced by fused filament fabrication. *Plastics, Rubber Compos.* 2018;47:17-24. doi:10.1080/14658011.2017.1399531
- Das A. Rheological investigation of nylon-carbon fiber composites fabricated using material extrusion-based additive manufacturing. *Polym Compos.* 2021;42:6010-6024. doi:10. 1002/pc.26281
- 98. Yu S, Bale H, Park S, Hwang JY, Hong SH. Anisotropic microstructure dependent mechanical behavior of 3D-printed basalt fiber-reinforced thermoplastic composites. *Compos Part B Eng.* 2021;224:109184. doi:10.1016/j.compositesb.2021.109184
- Consul P, Beuerlein KU, Luzha G, Drechsler K. Effect of extrusion parameters on short fiber alignment in fused filament fabrication. *Polymers*. 2021;13:1-24. doi:10.3390/polym13152443
- 100. Yan J, Demirci E, Ganesan A, Gleadall A. Extrusion width critically affects fibre orientation in short fibre reinforced material extrusion additive manufacturing. *Addit Manuf*. 2022;49:102496. doi:10.1016/j.addma.2021.102496
- 101. Yan J, Demirci E, Gleadall A. 3D short fibre orientation for universal structures and geometries in material extrusion additive manufacturing. *Addit Manuf*. 2023;69:103535. doi:10. 1016/j.addma.2023.103535
- 102. Yang D, Zhang H, Wu J, McCarthy ED. Fibre flow and void formation in 3D printing of short-fibre reinforced thermoplastic composites: an experimental benchmark exercise. *Addit Manuf.* 2021;37:101686. doi:10.1016/J.ADDMA.2020.101686
- 103. Fu Y-T, Li J, Guo FL, Li YQ, Fu SY. Micro-structure and tensile property analyses of 3D printed short carbon fiber

- reinforced PEEK composites. *Compos Commun.* 2023;41: 101655. doi:10.1016/j.coco.2023.101655
- 104. König M, Diekmann J, Lahres M, Middendorf P. Experimental investigation of process-structure effects on interfacial bonding strength of a short carbon fiber/polyamide composite fabricated by fused filament fabrication. *Prog Addit Manuf*. 2022;7:593-607. doi:10.1007/s40964-021-00249-4
- 105. Pei S, Wang K, Chen CB, et al. Process-structure-property analysis of short carbon fiber reinforced polymer composite via fused filament fabrication. *J Manuf Proc.* 2021;64:544-556. doi:10.1016/j.jmapro.2021.02.019
- 106. Tikhani F, Gurbin A, Hubert P. Unveiling the impact of short fibre reinforcement and extrusion properties on microstructure of 3D printed polycarbonate composites. *Addit Manuf*. 2024;93:104423. doi:10.1016/j.addma.2024.104423
- Sommacal S, Matschinski A, Holmes J, Drechsler K, Compston P. Detailed void characterisation by X-ray computed tomography of material extrusion 3D printed carbon fibre/PEEK. Compos Struct. 2023;308:116635. doi:10.1016/j. compstruct.2022.116635
- 108. Bellehumeur C, Li L, Sun Q, Gu P. Modeling of bond formation between polymer filaments in the fused deposition modeling process. *J Manuf Proc.* 2004;6:170-178. doi:10.1016/S1526-6125(04)70071-7
- 109. Garzon-Hernandez S, Garcia-Gonzalez D, Jérusalem A, Arias A. Design of FDM 3D printed polymers: an experimental-modelling methodology for the prediction of mechanical properties. *Mater Des.* 2020;188:108414. doi:10.1016/j.matdes.2019.108414
- 110. Sun Q, Rizvi GM, Bellehumeur CT, Gu P. Effect of processing conditions on the bonding quality of FDM polymer filaments. *Rapid Prototyping J.* 2008;14:72-80. doi:10.1108/13552540810862028
- Luo H, Yang H, Xi L, Liao B, Bo K. Effect of printing velocity on the microscopic void distribution of 3D-printed shortfiber-reinforced composites. *J Failure Anal Prevention*. 2022; 22:1085-1090. doi:10.1007/s11668-022-01399-5
- 112. Kubota M, Hayakawa K, Todoroki A. Effect of build-up orientations and process parameters on the tensile strength of 3D printed short carbon fiber/PA-6 composites. Adv Compos Mater. 2022;31:119-136. doi:10.1080/09243046.2021.1930497
- Coogan TJ, Kazmer DO. Prediction of interlayer strength in material extrusion additive manufacturing. *Addit Manuf*. 2020;35:101368. doi:10.1016/j.addma.2020.101368
- 114. Shafighfard T, Cender TA, Demir E. Additive manufacturing of compliance optimized variable stiffness composites through short fiber alignment along curvilinear paths. *Addit Manuf.* 2021;37:101728. doi:10.1016/j.addma.2020.101728
- 115. Spoerk M, Savandaiah C, Arbeiter F, et al. Anisotropic properties of oriented short carbon fibre filled polypropylene parts fabricated by extrusion-based additive manufacturing. *Compos Part A: Appl Sci Manuf.* 2018;113:95-104. doi:10.1016/j.compositesa.2018.06.018
- 116. Ferreira RTL, Amatte IC, Dutra TA, Bürger D. Experimental characterization and micrography of 3D printed PLA and PLA reinforced with short carbon fibers. *Compos B Eng.* 2017; 124:88-100. doi:10.1016/j.compositesb.2017.05.013
- Jiang D, Smith DE. Mechanical behavior of carbon fiber composites produced with fused filament fabrication. Conference: Solid Freeform Fabrication, Austin, Texas. 2016.

- 118. Mohankumar HR, Mohankumar HR, Benal MGM, et al. Effect of short glass fiber addition on flexural and impact behavior of 3D printed polymer composites. *ACS Omega*. 2023;8(10):9212-9220. doi:10.1021/acsomega.2c07227
- 119. Ning F, Cong W, Qiu J, Wei J, Wang S. Additive manufacturing of carbon fiber reinforced thermoplastic composites using fused deposition modeling. *Compos B Eng.* 2015;80:369-378. doi:10.1016/j.compositesb.2015.06.013
- 120. Liao G, Li Z, Cheng Y, et al. Properties of oriented carbon fiber/polyamide 12 composite parts fabricated by fused deposition modeling. *Mater Des.* 2018;139:283-292. doi:10.1016/j. matdes.2017.11.027
- 121. Lobov E, Dobrydneva A, Vindokurov I, Tashkinov M. Effect of short carbon fiber reinforcement on mechanical properties of 3D-printed acrylonitrile butadiene styrene. *Polymers*. 2023; 15:1-16. doi:10.3390/polym15092011
- 122. Kong X, Sun G, Luo Q, Brykin V, Qian J. Experimental and theoretical studies on 3D printed short and continuous carbon fiber hybrid reinforced composites. *Thin-Wall Struct.* 2024; 205:112406. doi:10.1016/j.tws.2024.112406
- Ding Q, Li X, Zhang D, Zhao G, Sun Z. Anisotropy of poly(lactic acid)/carbon fiber composites prepared by fused deposition modeling. *J Appl Polym Sci.* 2020;137:1-11. doi:10. 1002/app.48786
- 124. Chen J, Liu X, Tian Y, et al. 3D-printed anisotropic polymer materials for functional applications. *Adv Mater.* 2022;34: e2102877. doi:10.1002/adma.202102877
- 125. Lv X, Yang S, Pei X, Zhang Y, Wang Q, Wang T. Tribological anisotropy of PEEK composites filled with highly oriented carbon fibers manufactured by fused deposition modeling. *Polym Compos.* 2024;45(3):2656-2669. doi:10.1002/pc.27946
- 126. Zhang W, Cotton C, Sun J, et al. Interfacial bonding strength of short carbon fiber/acrylonitrile-butadiene-styrene composites fabricated by fused deposition modeling. *Compos B Eng.* 2018;137:51-59. doi:10.1016/j.compositesb.2017.11.018
- 127. Távara L, Madrigal C, Aranda MT, Justo J. Anisotropy and ageing effect on the mechanical behaviour of 3D-printed short carbon-fibre composite parts. *Compos Struct*. 2023;321:117196. doi:10.1016/j.compstruct.2023.117196
- 128. Srinivasan Ganesh Iyer S, Keles O. Effect of raster angle on mechanical properties of 3D printed short carbon fiber reinforced acrylonitrile butadiene styrene. *Compos Commun*. 2022;32:101163. doi:10.1016/j.coco.2022.101163
- 129. Yan J, Demirci E, Gleadall A. Single-filament-wide tensile-testing specimens reveal material-independent fibre-induced anisotropy for fibre-reinforced material extrusion additive manufacturing. *Rapid Prototyping J.* 2023;29:1453-1470. doi: 10.1108/RPJ-09-2022-0301
- 130. Allum J, Moetazedian A, Gleadall A, Silberschmidt VV. Interlayer bonding has bulk-material strength in extrusion additive manufacturing: new understanding of anisotropy. *Addit Manuf.* 2020;34:101297. doi:10.1016/j.addma.2020.101297
- 131. Bhandari S, Lopez-Anido RA, Gardner DJ. Enhancing the interlayer tensile strength of 3D printed short carbon fiber reinforced PETG and PLA composites via annealing. Addit Manuf. 2019;30:100922. doi:10.1016/j.addma.2019.100922
- 132. Wang Z, Luan C, Liao G, Yao X, Fu J. Mechanical and self-monitoring behaviors of 3D printing smart continuous carbon

- fiber-thermoplastic lattice truss sandwich structure. *Compos B Eng.* 2019;176:107215. doi:10.1016/j.compositesb.2019.107215
- 133. Duty C, Failla J, Kim S, Smith T, Lindahl J, Kunc V. Z-pinning approach for 3D printing mechanically isotropic materials. Addit Manuf. 2019;27:175-184. doi:10.1016/j.addma.2019. 03.007
- 134. Kara Y, Kovács NK, Nagy-György P, Boros R, Molnár K. A novel method and printhead for 3D printing combined nano—/microfiber solid structures. *Addit Manuf.* 2023;61: 103315. doi:10.1016/j.addma.2022.103315
- 135. Jin M, Neuber C, Schmidt HW. Tailoring polypropylene for extrusion-based additive manufacturing. *Addit Manuf.* 2020; 33:101101. doi:10.1016/j.addma.2020.101101
- 136. Xu Q, Xu W, Yang Y, et al. Enhanced interlayer strength in 3D printed poly (ether ether ketone) parts. *Addit Manuf.* 2022; 55:102852. doi:10.1016/j.addma.2022.102852
- 137. Park SJ, Kim DH, et al. Increased interlayer bonding strength of short carbon fiber composite fabricated by material extrusion via warm isostatic pressing (WIP) process. *J Mater Res Technol.* 2023;25:3610-3623. doi:10.1016/j.jmrt.2023.06.130
- 138. Abbott AC, Tandon GP, Bradford RL, Koerner H, Baur JW. Process-structure-property effects on ABS bond strength in fused filament fabrication. *Addit Manuf.* 2018;19:29-38. doi: 10.1016/j.addma.2017.11.002
- 139. Zhou M, Zhou X, Si L, et al. Modeling of bonding strength for fused filament fabrication considering bonding interface evolution and molecular diffusion. *J Manuf Proc.* 2021;68:1485-1494. doi:10.1016/j.jmapro.2021.06.064
- 140. Chacón JM, Caminero MA, García-Plaza E, Núñez PJ. Additive manufacturing of PLA structures using fused deposition modelling: effect of process parameters on mechanical properties and their optimal selection. *Mater Des.* 2017;124:143-157. doi:10.1016/j.matdes.2017.03.065
- 141. Mishurova T, Rachmatulin N, Fontana P, et al. Evaluation of the probability density of inhomogeneous fiber orientations by computed tomography and its application to the calculation of the effective properties of a fiber-reinforced composite. *Int J Eng Sci.* 2018;122:14-29. doi:10.1016/j.ijengsci.2017.10.002
- 142. Chin W-K, Liu HT, Lee YD. Effects of fiber length and orientation distribution on the elastic modulus of short fiber reinforced thermoplastics. *Polym Compos.* 1988;9:27-35. doi:10. 1002/pc.750090105
- 143. Hine PJ, Rudolf Lusti H, Gusev AA. Numerical simulation of the effects of volume fraction, aspect ratio and fibre length distribution on the elastic and thermoelastic properties of short fibre composites. *Compos Sci Technol*. 2002;62:1445-1453. doi:10.1016/S0266-3538(02)00089-1
- 144. Petrény R, Tóth C, Horváth A, Mészáros L. Development of electrically conductive hybrid composites with a poly(lactic acid) matrix, with enhanced toughness for injection molding, and material extrusion-based additive manufacturing. *Heli*yon. 2022;8:e10287. doi:10.1016/j.heliyon.2022.e10287
- 145. Shemelya C, de la Rosa A, Torrado AR, et al. Anisotropy of thermal conductivity in 3D printed polymer matrix composites for space based cube satellites. *Addit Manuf.* 2017;16:186-196. doi:10.1016/j.addma.2017.05.012
- 146. Nikolaou C, Polyzos E, Zhu Y, Polyzos D, Pyl L. Modeling of 3D-printed composite filaments using X-ray computer

15480569, 0, Downloaded from https://4spepublications.onlinelibrary.wiley.com/doi/10.1002/pc.29850 by Budapest University of Technology and Economics, Wiley Online Library on [21/08/2025]. See the Terms and Conditions (https://onlinelibrary.wiley

ditions) on Wiley Online Library for rules of use; OA articles are governed by the applicable Creative Commons

- tomography images segmented by neural networks. *Addit Manuf.* 2024;85:104181. doi:10.1016/j.addma.2024.104181
- 147. Fu S-Y, Lauke B, Mai YW. Major factors affecting the performance of short fibre reinforced polymers. *Sci Eng Short Fibre Reinf Polym Compos.* 2009:29-58. doi:10.1533/9781845696498.29
- 148. Bodaghi M, Cristóvão C, Gomes R, Correia NC. Experimental characterization of voids in high fibre volume fraction composites processed by high injection pressure RTM. *Compos Part A: Appl Sci Manuf.* 2016;82:88-99. doi:10.1016/j. compositesa.2015.11.042
- 149. Huang D, Zhao X. Novel modified distribution functions of fiber length in fiber reinforced thermoplastics. *Compos Sci Technol*. 2019;182:107749. doi:10.1016/j.compscitech.2019. 107749
- 150. Li Y, Li W, Deng Y, et al. Temperature-dependent longitudinal tensile strength model for short-fiber-reinforced polymer composites considering fiber orientation and fiber length distribution. *J Mater Sci.* 2018;53:12190-12202. doi:10.1007/s10853-018-2517-8
- Barbero EJ. Introduction to Composite Materials Design. 3rd ed. CRC Press; 2017.
- 152. Sayah N, Smith DE. Effect of process parameters on void distribution, volume fraction, and Sphericity within the bead microstructure of large-area additive manufacturing polymer composites. *Polymers*. 2022;14:1-18. doi:10.3390/polym14235107
- 153. Li L, Sun Q, Bellehumeur C, Gu P. Composite modeling and analysis for fabrication of FDM prototypes with locally controlled properties. *J Manuf Proc.* 2002;4:129-141. doi:10.1016/ S1526-6125(02)70139-4
- 154. Papon EA, Haque A, Mulani SB. Process optimization and stochastic modeling of void contents and mechanical properties in additively manufactured composites. *Compos B Eng.* 2019;177:107325. doi:10.1016/j.compositesb.2019.107325
- Obaid N, Kortschot M, Sain M. Understanding the stress relaxation behavior of polymers reinforced with short elastic fibers. *Materials*. 2017;10. doi:10.3390/ma10050472
- 156. Yan J, Demirci E, Gleadall A. Are classical fibre composite models appropriate for material extrusion additive manufacturing? A thorough evaluation of analytical models. *Addit Manuf.* 2023;62:103371. doi:10.1016/J.ADDMA.2022. 103371
- 157. Zou R, Xia Y, Liu S, et al. Isotropic and anisotropic elasticity and yielding of 3D printed material. *Compos B Eng.* 2016;99: 506-513. doi:10.1016/j.compositesb.2016.06.009
- 158. Mishra N, Das K. A Mori–Tanaka based micromechanical model for predicting the effective Electroelastic properties of orthotropic piezoelectric composites with spherical inclusions. SN Appl Sci. 2020;2:1-14. doi:10.1007/s42452-020-2958-y
- 159. Yan X, Yang Y, Hamada H. Tensile properties of glass fiber reinforced polypropylene composite and its carbon fiber hybrid composite fabricated by direct fiber feeding injection molding process. *Polym Compos.* 2018;39:3564-3574. doi:10.1002/pc. 24378
- 160. Junaedi H, Baig M, Dawood A, Albahkali E, Almajid A. Modeling analysis of the tensile strength of polypropylene base short carbon fiber reinforced composites. *J Mater Res Technol.* 2021;11:1611-1621. doi:10.1016/j.jmrt.2021.02.010
- 161. Gonabadi H, Chen Y, Bull S. Investigation of the effects of volume fraction, aspect ratio and type of fibres on the

- mechanical properties of short fibre reinforced 3D printed composite materials. *Prog Addit Manuf.* 2024;10(1):261-277. doi:10.1007/s40964-024-00620-1
- 162. Estefani A, Távara L. Numerical multiscale analysis of 3D printed short fiber composites parts: filament anisotropy and toolpath effects. *Eng Reports*. 2024;6:1-16. doi:10.1002/eng2. 12799
- 163. Bandinelli F, Scapin M, Peroni L. Effects of anisotropy and infill pattern on compression properties of 3D printed CFRP: mechanical analysis and elasto-plastic finite element modelling. *Rapid Prototyping J.* 2024;30:142-158. doi:10.1108/RPJ-11-2023-0385
- 164. Cai H, Ye J, Wang Y, et al. An effective microscale approach for determining the anisotropy of polymer composites reinforced with randomly distributed short fibers. *Compos Struct*. 2020;240:112087. doi:10.1016/j.compstruct.2020.112087
- 165. Lei M, Wang Y, Wei Q, Li M, Zhang J, Wang Y. Micromechanical modeling and numerical homogenization calculation of effective stiffness of 3D printing PLA/CF composites. *J Manuf Proc.* 2023;102:37-49. doi:10.1016/j.jmapro.2023.07.027
- 166. Yan Z, Rahimizadeh A, Zhang Y, Zhou Y, Lessard L. A finite element model for 3D printed recycled parts from end-of-life wind turbine blades. *Compos Struct*. 2023;320:117177. doi:10. 1016/j.compstruct.2023.117177
- 167. Tóth C, Kovács NK. Comparison of the accuracy of analytical models for basalt fiber–reinforced poly(lactic acid) composites prepared by injection molding and fused filament fabrication. *Int J Adv Manuf Technol.* 2022;121:3999-4010. doi:10.1007/ s00170-022-09572-8
- 168. Shirasu K, Yamaguchi Y, Hoshikawa Y, Kikugawa G, Tohmyoh H, Okabe T. Micromechanics study of short carbon fiber-reinforced thermoplastics fabricated via 3D printing using design of experiments. *Mater Sci Eng A*. 2024;891: 145971. doi:10.1016/j.msea.2023.145971
- 169. Gupta A, Hasanov S, Fidan I, Zhang Z. Homogenized modeling approach for effective property prediction of 3D-printed short fibers reinforced polymer matrix composite material. *Int J Adv Manuf Technol*. 2022;118:4161-4178. doi:10.1007/s00170-021-08230-9
- 170. Somireddy M, Singh CV, Czekanski A. Mechanical behaviour of 3D printed composite parts with short carbon fiber reinforcements. *Eng Failure Anal.* 2020;107:104232. doi:10.1016/j.engfailanal.2019.104232
- Pemas S, Gkiliopoulos D, Samiotaki C, et al. Valorization of tomato agricultural waste for 3D-printed polymer composites based on poly(lactic acid). *Polymers*. 2024;16:1-18. doi:10. 3390/polym16111536
- 172. Yu IKM, Chan OY, Zhang Q, Wang L, Wong KH, Tsang DCW. Upcycling of spent tea leaves and spent coffee grounds into sustainable 3D-printing materials: natural plasticization and low-energy fabrication. *ACS Sustain Chem Eng.* 2023;11:6230-6240. doi:10.1021/acssuschemeng.2c07330
- 173. Li S, Shi C, Sun S, et al. From brown to colored: Polylactic acid composite with micro/nano-structured white spent coffee grounds for three-dimensional printing. *Int J Biol Macromol*. 2021;174:300-308. doi:10.1016/j.ijbiomac.2021.01.176
- 174. Boughanmi O, Allegue L, Marouani H, Koubaa A, Fouad Y. Repetitive recycling effects on mechanical characteristics of poly-lactic acid and PLA/spent coffee grounds composite used

- for 3D printing filament. *Polym Eng Sci.* 2024;64(11):5613-5626. doi:10.1002/pen.26938
- 175. Morales MA, Atencio Martinez CL, et al. Development and characterization of rice husk and recycled polypropylene composite filaments for 3d printing. *Polymers*. 2021;13:1-17. doi: 10.3390/polym13071067
- 176. Rojas-Martínez LE, Flores-Hernandez CG, López-Marín LM, et al. 3D printing of PLA composites scaffolds reinforced with keratin and chitosan: effect of geometry and structure. *Eur Polym J.* 2020;141:110088. doi:10.1016/j. eurpolymj.2020.110088
- 177. Sotohou F, Mwangi JW, Mutua JM, Ronoh EK. Development and evaluation of recycled polypropylene and bean pod powder composite biomaterial for fused filament fabrication. *Adv Mater Phys Chem.* 2023;13:31-48. doi:10.4236/ampc.2023.
- 178. Idrees M, Jeelani S, Rangari V. Three-dimensional-printed sustainable biochar-recycled PET composites. *ACS Sustain Chem Eng.* 2018;6(11):13940-13948. doi:10.1021/acssusch emeng.8b02283
- 179. Mohammed Z, Jeelani S, Rangari V. Effective reinforcement of engineered sustainable biochar carbon for 3D printed polypropylene biocomposites. *Compos Part C: Open Access*. 2022; 7:100221. doi:10.1016/j.jcomc.2021.100221
- 180. Vidakis N, Petousis M, Kalderis D, et al. Reinforced HDPE with optimized biochar content for material extrusion additive manufacturing: morphological, rheological, electrical, and thermomechanical insights. *Biochar*. 2024;6:1-21. doi:10.1007/s42773-024-00314-5
- 181. Hassan M, Mohanty AK, Misra M. 3D printing in upcycling plastic and biomass waste to sustainable polymer blends and composites: a review. *Mater Des.* 2024;237:112558. doi:10. 1016/j.matdes.2023.112558
- 182. Carmona-Cabello M, Herreros JM, Molero E, et al. Upcycling of agricultural residues for additive manufacturing: corn straw waste as reinforcing agent in acrylonitrile-butadiene-styrene composite matrix. *Biomass Convers Biorefinery*. 2024;15(5): 7869-7880. doi:10.1007/s13399-024-05639-6
- 183. Nguyen HT, Crittenden K, Weiss L, Bardaweel H. Recycle of waste tire rubber in a 3D printed composite with enhanced damping properties. *J Clean Prod.* 2022;368:133085. doi:10. 1016/j.jclepro.2022.133085
- 184. Yusuf Y, Mustafa N, Yusoff YF, Sulistyarini DH. The mechanical and physical properties of 3D printing filament made from recycled polypropylene and ground Tyre rubber treated with alkali. *Pertanika J Sci Technol.* 2024;32:151-163. doi:10. 47836/pjst.32.S2.10
- 185. Badini S, Graziosi S, Carboni M, Regondi S, Pugliese R. Sustainable 3D printing with recycled tire rubber-based filaments: an investigation of process parameters and mechanical behaviour. *Rapid Prototyping J.* 2024;30:571-587. doi:10.1108/RPJ-08-2023-0309
- 186. Gama N, Ferreira A, Barros-Timmons A. 3D printed thermoplastic polyurethane filled with polyurethane foams residues. *J Polym Environ*. 2020;28:1560-1570. doi:10.1007/s10924-020-01705-y
- 187. Gaikwad V, Ghose A, Cholake S, Rawal A, Iwato M, Sahajwalla V. Transformation of E-waste plastics into

- sustainable filaments for 3D printing. *ACS Sustain Chem Eng.* 2018;6:14432-14440. doi:10.1021/acssuschemeng.8b03105
- 188. Spirio A, Arrigo R, Frache A, Tuccinardi L, Tuffi R. Plastic waste recycling in additive manufacturing: recovery of polypropylene from WEEE for the production of 3D printing filaments. *J Environ Chem Eng.* 2024;12:112474. doi:10.1016/j.jece.2024.112474
- 189. Rahimizadeh A, Kalman J, Fayazbakhsh K, Lessard L. Mechanical and thermal study of 3D printing composite filaments from wind turbine waste. *Polym Compos.* 2021;42(5): 2305-2316. doi:10.1002/pc.25978
- 190. Ezhilan JJ, Damodaran A, Ashok KG. Decentralized approach for incorporating waste wind turbine blades into 3D printing filaments using mechanical recycling. *Polym Compos*. 2024; 46(3):2319-2332. doi:10.1002/pc.29107
- 191. Wei B, Yang S, Wang Q. Green recycling of aluminum plastic packaging waste by solid-state shear milling and 3D printing for thermal conductive composites. *Polymers Adv Technol.* 2021;32(6):2576-2587. doi:10.1002/pat.5289
- 192. Carrete IA, Quiñonez PA, Bermudez D, Roberson DA. Incorporating textile-derived cellulose fibers for the strengthening of recycled polyethylene terephthalate for 3D printing feed-stock materials. *J Polym Environ*. 2021;29:662-671. doi:10. 1007/s10924-020-01900-x
- 193. Haque ANMA, Naebe M, Mielewski D, Kiziltas A. Waste wool/polycaprolactone filament towards sustainable use in 3D printing. *J Clean Prod.* 2023;386:135781. doi:10.1016/j. iclepro.2022.135781
- 194. Zhu B, Wang Y, Sun J, et al. An experimental study on the influence of waste rubber particles on the compressive, flexural and impact properties of 3D printable sustainable cementitious composites. *Case Studies Constr Mater.* 2023;19:e02607. doi:10.1016/j.cscm.2023.e02607
- 195. Joyee EB, Lu L, Pan Y. Analysis of mechanical behavior of 3D printed heterogeneous particle-polymer composites. *Compos B Eng.* 2019;173:106840. doi:10.1016/j.compositesb.2019.05.051
- Rooney K, Dong Y, Basak AK, Pramanik A. Prediction of mechanical properties of 3D printed particle-reinforced resin composites. *J Compos Sci.* 2024;8:1-40. doi:10.3390/jcs8100416
- 197. Papon EA, Haque A, Spear SK. Effects of functionalization and annealing in enhancing the interfacial bonding and mechanical properties of 3D printed fiber-reinforced composites. *Mater Today Commun.* 2020;25:101365. doi:10.1016/j.mtcomm.2020.101365

## SUPPORTING INFORMATION

Additional supporting information can be found online in the Supporting Information section at the end of this article.

**How to cite this article:** Tóth C, Molnár K, Virág ÁD. Short fiber reinforcement in material extrusion 3D printing: A meta-analysis review with insights into sustainable alternatives. *Polym Compos.* 2025;1-39. doi:10.1002/pc.29850